IMPLICATIONS OF WATER-ROCK REACTIONS IN LAVA TUBE ENVIRONMENTS AT LAVA BEDS NATIONAL MONUMENT

BY

JESSICA PELUSO

A THESIS SUBMITTED IN PARTIAL FULFILLMENT OF THE REQUIREMENTS FOR THE DEGREE OF

MASTER OF SCIENCE

IN

BIOLOGICAL AND ENVIRONMENTAL SCIENCES

UNIVERSITY OF RHODE ISLAND

2024

MASTER OF SCIENCE THESIS

OF

JESSICA PELUSO

APPROVED:

Thesis Committee:

Major Professor Dawn Cardace

Soni Pradhanang

Irene Andreu

Brenton DeBoef
DEAN OF THE GRADUATE SCHOOL

UNIVERSITY OF RHODE ISLAND
2024

ABSTRACT

Lava caves are widespread in volcanic terrains on Earth and other worlds, containing metal-rich rock compositions that attract life and react with waters in dark and secluded environments. Water-rock reactions in these settings promote alteration of the basalt substrate and initiate the formation of secondary minerals in addition to colonization by microbes. The varieties of secondary minerals present in lava caves can serve as indicators of weathering types, previous environmental conditions, reaction progress, and may even be useful in preserving potential biosignatures. Secondary mineral samples from lava caves at Lava Beds National Monument were collected and analyzed with X-ray diffraction (XRD) and Fourier Transform Infrared Spectroscopy (FTIR) to determine their mineralogy. Geochemical modeling of similar basalt and groundwater interactions, using the Geochemist's Workbench, was conducted to compare with field-based findings. Carbonate and clay minerals were abundant amongst samples collected in the field and were predicted in model outputs in the initial stages of the reaction. This indicates water-rock reactions at Lava Beds National Monument are still ongoing, have yet to reach thermodynamic equilibrium, and may provide energy to microbes living within the caves. Since lava caves are present on other worlds and are sheltered from environmental stresses through time, they are ideal astrobiological targets where minerals, microbes or biosignatures may be found.

ACKNOWLEDGMENTS

I would like to express my deepest appreciation to my M.S. thesis adviser Dr. Dawn Cardace for her continued support and guidance over the past three years. Additionally, I am thankful to the many faculty, staff, and fellow graduate students at the University of Rhode Island across departments for their constant friendship and encouragement. This endeavor would not have been possible without the generous support from the NASA Rhode Island Space Grant Consortium, an agency I extend sincere thanks to.

I acknowledge David L. Hays, the Natural Resources Manager at Lava Beds National Monument, for his help and support in attaining a sample collection permit from the National Park Service. I would also like to recognize the contributions of NASA Space Grant 2023 summer intern Wilnelia Barea Carrion for her help in the preparation and analysis of samples described herein. I had the pleasure of working with several mentors within the URI College of Engineering core facility who were instrumental in the acquisition of spectral data for this work.

Lastly, I thank my family and friends for their unwavering support as I established myself professionally and personally within the state of Rhode Island, a place that has not only inspired my scientific research but become my second home.

PREFACE

This thesis is in Manuscript Format, prepared for submission to the scientific journal *Icarus*.

TABLE OF CONTENTS

LIST OF TABLES

TABLE PAGE

LIST OF FIGURES

FIGURE PAGE

MANUSCRIPT – 1

Prepared for publication in Icarus journal

Implications of Water-Rock Reactions in Lava Tube Environments at Lava Beds National Monument

Jessica Peluso

Department of Geosciences

University of Rhode Island, RI USA

Corresponding Author: Dawn Cardace, Ph.D.

Department of Geosciences

University of Rhode Island

490 CBLS

120 Flagg Road

Kingston, RI, 02881, USA

Phone: +1 (401) 874-9384

Email: cardace@uri.edu

Key Terms: Mars analogue, mineralogy, x-ray diffraction, FTIR spectroscopy, biofilm characterization.

INTRODUCTION

The presence of liquid water on Mars's surface in the past has been proven by the identification of fluvial geomorphological features such as fans, river channels, gullies and layered sediments (Schulze-Makuch et al., 2008). Hydrated alteration minerals such as phyllosilicates and sulfates have also been detected across the planet suggesting widespread liquid water exposure and its contact with igneous rocks (Poulet et al., 2005, Mangold et al., 2007). Such reactions may also be of astrobiological significance.

Though early Mars had conditions favorable for life, the surface of modern Mars hosts a likely barren, extreme environment that is thought to make the surface inhospitable, even for resilient microbes. Extreme fluctuations in temperature, bombardment by micrometeoroids and high doses of radiation would be too great for organisms or evidence of their biosignatures to withstand (Kminek and Bada, 2006, Hassler et al. 2014, Cheptsov et al., 2018). Because of this, many studies over the past decade have shifted their attention to the subsurface when looking for signs of life on Mars.

The two most powerful forms of radiation on Mars are solar-derived energetic particles and galactic cosmic rays, both of which can reach and penetrate up to three meters into the regolith (Hassler et al., 2014). Along with providing protection from radiation, the subsurface may also house deposits of water ice (Williams et al., 2010, Cushing, 2012, Schorghofer, 2021). This water ice may be the product of condensation and accumulation rates that exceed those of sublimation, or it may be remnant from an earlier time with a

more temperate climate (Cushing, 2012, Schorghofer, 2021). It is also theorized that small amounts of liquid water may be present on rocks in the subsurface in the form of thin films or brine pockets, where they are shielded from sublimation and relict from when Mars had more significant surface water (Schulze-Makuch et al., 2008). The rock-water interactions that may occur on these interfaces could prove promising for the development of simple life such as biofilms, especially if the rock substrate has a chemical composition favorable to the biofilm's metabolism. Several studies have proven that biofilms preferentially colonize surfaces with high content of metals, particularly iron (Rogers and Bennet, 2004, Scholl et al., 1990).

Mars hosts an extensive network of rock cavities, the most prominent of which were created by lava flows. Lava caves originally formed as lava flows traveled in long sinuous paths at the surface. The exterior of the tube cooled and solidified while the hot lava in the center continued along its irregular path. When the eruption ends and the supply of lava is exhausted, the solidified outer rim forms a cavity in the conduit-like path of the lava. Several entrances [in the form of skylights] to lava caves on Mars have been photographed and identified for future exploration, with many occurring in the Tharsis region (Cushing et al., 2007, Cushing, 2012), a volcanic area that dominates the planet's western hemisphere

The interaction of fluid with rocks in the subsurface spurs the biotic and abiotic alteration of existing minerals and the precipitation of secondary minerals, which are excellent reservoirs for preserving biosignatures (Hays et

al., 2017). Such biosignatures may include microbe induced minerals containing structural features distinctly indicative of biological formation (Cady and Farmer, 1996) or biological compounds that could be entrapped within the secondary mineral deposits (Boston et al., 2001). Terrestrial rock cavities, especially those exposed to water, often exhibit water/rock interface colonization in the form of surface biofilm and/or endolithic biological colonization which can cause weathering of the rock surface (Roldan and Hernandez-Marine, 2009, Northup et al., 2011, Sallstedt et al., 2014, Hays et al., 2017, Popovic et al., 2021). If water (as liquid or ice) exists within cavities of the Tharsis region, extant life could feasibly lead to biofilm colonization or biologically mediated weathering of their surfaces.

Biofilms are composed of one or several species and layers of microorganisms. These groupings exist within a slimy mix of extracellular polymeric substances that allow the organisms to stay hydrated, acquire resources, protect themselves, and adhere easily to surfaces (Fleming et al., 2016). Under laboratory conditions biofilms have been desiccated then rehydrated showing limited distress, proving they can endure for long periods of time with minimal exposure to water (Billi et al., 2011, Baque et al., 2013, Billi, 2018, Billi et al., 2019, Mosca et al., 2019). Biofilms have also been experimentally exposed to radiation equivalent to that of the Martian surface and near subsurface, providing evidence that even the shallow subsurface can provide protection from radiation for prolonged amounts of time (Billi et al., 2011; Billi, 2018). Billi et al. (2019) also suggests that in layered biofilms, even

if the topmost exposed layers are bleached from UV exposure, the underlying layers can remain alive and unharmed. In an experiment that exposed biofilms to extreme UV flux levels similar to the early Earth, some biofilms, while not able to continue normal cell function, were able to survive in a dormant state for extended periods of time (Cockell et al., 2011). These characteristics make biofilms prime targets for life within the Martian subsurface as they could withstand conditions of high radiation and little water.

In this study, numerous sampling sites in Mars analog lava caves at Lava Beds National Monument, in Tulelake, CA, were investigated for co-occurring secondary minerals, biologically derived compounds, and microbial diversity. A map of the study area, a photo from the inside of a lava cave and an example of their unique basalt textures are shown in Figure 1. The region is dominated by several basalt flows, most of which originate from the Mammoth and Modoc craters with some flows as young as 1,100 years old. Interpreting data for co-registered mineralogy and microbiology in these unique settings, the following hypotheses are tested:

1/ Initial (primary rock-forming) and alteration (secondary) minerals differ from each other, and are consistent with expected low temperature, oxidative basalt alteration processes;

2/ Alteration minerals correspond to specific stages of the water-rock reaction path, and therefore have indicative power for assessing reaction progress and changing Eh/pH/ion activity, and pore scale habitability;

3/ Martian lava cave mineral-hosted biosignatures have variable preservation potential due to differing mineral stabilities, thus it is possible to rank order minerals to target for biosignature detection.

METHODS

2.1.1 Sample collection procedure

Rock, mineral, and biology samples were collected in lava tubes/lava caves at Lava Beds National Monument. Caves selected for sampling include Hopkins Chocolate, Valentine and Golden Dome, which were chosen to leverage accessibility and prior characterization by Lavoie et al. (2017) and Kulkarni et al. (2022). Initial surveys were conducted to locate deposits of secondary minerals or areas with dense biofilm colonization. Mineral and biology samples were later acquired in these heavily altered and colonized areas. Unaltered samples of the cave rock were collected from the walls of Hopkins Chocolate and Valentine cave in areas that appeared dry and consistent in color with unreacted basalt. The unaltered samples were acquired from loose pieces of basaltic a'a from the cave walls and were promptly placed in labeled plastic bags. Samples from the two caves were labeled as HC unaltered and VAL unaltered.

Areas in the caves where the wall rock appeared different in texture or color from the surrounding basalt rock were considered altered, with potential secondary minerals. Secondary mineral colors observed included white, gray, tan, yellow and pink (Figure 2). A chisel and rock hammer were cleaned with isopropyl alcohol between sampling sites and used to remove several 1 to 3

cm sized pieces of secondary minerals from localized areas on the Hopkins Chocolate and Valentine cave walls. Upon their removal from the cave walls, mineral samples were placed in sterile plastic bags and labeled with the corresponding cave name, location, color and sample number. Five altered samples were collected within Hopkins Chocolate cave (HC sample 1, 2, 3, 4, and 5). Three altered samples were collected within Valentine cave (VAL 1, 2, and 3); photographs of these altered samples can be seen in Figure 2.

Biological samples were collected within Valentine and Golden Dome caves. In each, areas of dense biofilm colonization were identified and sampled. Two Zymo Research brand DNA/RNA shield collection tubes (2 ml volumes) with swab kits were used to collect biofilm samples at the chosen site within each cave. A gloved hand removed the sterile swab from its packaging and promptly wiped stalactites and/or areas on the cave ceiling or walls where biofilm was present. Swabbing took place for approximately 10 seconds and resulted in white or yellow gelatinous biofilm accumulating on the swab head. Once an appropriate amount of sample was collected on the swab, the swab head was placed into the collection tube, covered with reagent. Stainless steel (SS) scoopulas were sanitized with isopropyl alcohol prior to use and were used to scrape a greater volume of biofilm off of the wall/ceiling and directly into clean, sterile microcentrifuge tubes at each of the biology sampling sites, yielding one tube of biofilm from each of the Valentine and Golden Dome caves. All biology samples were stored in an icebox while at the field site,

were promptly shipped back to the laboratory on blue ice and were stored at -20 degrees C upon their return to the laboratory.

2.1.2 Ethics statement

The National Park Service oversees Lava Beds National Monument and recognizes it as a federally protected area. All sampling for this study was completed under Permit LABE-2023-SCI-0001 issued to Peluso by the National Park Service (Lava Beds National Monument, 1 Indian Well Headquarters, PO box 1240, Tulelake, CA 96134).

2.2 Modeling

The Geochemist's Workbench (GWB) software version 12.0 in REACT mode was used to model geochemical interactions between percolating meteoric water and regional basalt simulating the Lava Beds National Monument cave environment. The formation of secondary minerals and evolved waters within the caves was predicted. Solute activity is calculated within GWB's REACT mode using the Debye-Hückel equation, where the activity coefficient for each ion at each reaction step is determined based on concentrations of ions in the solution and the geochemical surroundings.

$$\log \gamma_i = - \frac{A z_i^2 \sqrt{I}}{1 + å_i B \sqrt{I}}$$

As shown here, Debye- Hückel determines the log of the activity coefficient (γ_i) using temperature functions (A and B), ion charge (z_i), solution ionic strength (I), and the ion size parameter ($å_i$) (Bethke, 2011).

Basalt modal mineralogy based on bulk rock geochemistry is well constrained (Hart et al., 1984) and mineral proportions were entered as fractions of one free kilogram of reactant. Lava Beds National Monument basalt is equivalent to 0.18 kg forsterite, 0.06 kg fayalite, 0.02 kg diopside, 0.03 kg enstatite, 0.47 kg anorthite, and 0.06 kg magnetite (Hart et al., 1984). Based on field reports and related analytical data, water sampled at Lava Beds National Monument is a Na^{+}-HCO_3^{-} type water at pH 6.7 at ambient cave temperature of 12 ± 4 degrees C, with 22 mg/L dissolved Si (Kulkarni et al., 2022). Mineral and water inputs for the Geochemist's Workbench are shown in Tables 1 and 2. A flowchart describing the model framework including model inputs and outputs is shown in Figure 3. The reaction was run at 12 degrees C as in the cool cave environment. The mineral species listed as saturated at different stages of the reaction progress were documented. Minerals at saturation are in equilibrium with the co-occurring aqueous solutions, and dissolve at the same rate as they form. Supersaturated minerals are expected to precipitate. Tracking both is a strategy for monitoring which secondary minerals should persist through time in the cave environment.

2.3 Analytical Methods

2.3.1 Sample Preparation

All rock and mineral samples collected in Hopkins Chocolate and Valentine caves were prepared for X-ray diffraction (XRD) and Fourier Transform Infrared spectroscopy (FTIR) analysis. The HC and VAL unaltered samples were broken into smaller 1 to 2 cm sized pieces using a sterile rock hammer

and crushed using a porcelain mortar and pestle. Mortar and pestle were cleaned with isopropyl alcohol between uses. The crushed material was then placed into a stainless steel 150 micron sieve (or 100 mesh) to isolate particles less than 150 microns. The outer surfaces of each altered sample were scraped with a sterilized SS scoopula to remove the secondary mineral coating. The removed coating was reduced using a porcelain mortar and pestle then sieved until particles were smaller than 150 microns. The sieved material from each of the unaltered and altered samples was placed in aluminum foil holding trays and dried in an oven at 55 degrees C for 12 hours to remove moisture. Dried samples were transferred from the aluminum trays to microcentrifuge tubes prior to analysis.

Samples of yellow biofilm collected in the Golden Dome and Valentine caves were prepared for FTIR analysis. One microcentrifuge worth of biofilm from each cave was lyophilized for 12 hours at -84 degrees C.

2.3.2 XRD

All samples were analyzed using the InXitu (now Olympus) Terra 213 X-ray diffractometer in the Cardace Laboratory/Department of Geosciences, College of the Environment and Life Sciences, University of Rhode Island, Kingston RI. This miniaturized XRD unit, modeled after the NASA CheMin instrument designed for Mars Science Laboratory mission, is outfitted with a cobalt anode (representative Co Kα X-rays have an energy of 6.929 keV; Blake et al., 2012). Powdered samples were loaded sequentially into the vibrating sample cell of the X-ray diffractometer. 1000 exposures from each sample were

collected. All X-ray diffraction data were downloaded from the Terra 213 interface as .plv files and analyzed within XPowder software version 2010.01.06 PRO. Background subtraction was applied to each diffractogram before interpretation. The altered samples, HC samples 1 to 5 and VAL samples 1 to 3, were compared to their respective unaltered samples to determine if noticeable differences existed. A mineral identification peak database was used to identify peaks within the unaltered and altered diffractograms resulting in the documentation of mineral names, corresponding d values, and Miller indices. Peaks common to HC and VAL unaltered samples confirmed the primary minerals of the cave basalt. Different peak sets in the diffractograms of altered samples were diagnostic for secondary minerals.

2.3.3 FTIR

XRD samples were subsequently analyzed with a Shimadzu IRTracer-100 FTIR spectrometer in Attenuated Total Reflectance (ATR) mode in the RIN2 Nanomaterials Laboratory, College of Engineering, University of Rhode Island, Kingston RI. ATR mode uses the single reflection QATR 10 accessory. The instrument is controlled through the LabSolutionsIR software interface where instrument settings can be specified, and the spectra can be viewed or manipulated. 200 scans were completed for each sample scan. Measurements were acquired in percent transmittance mode with a Happ-Genzel apodization and a resolution of 8. The range of data collection was 500-4000 cm^{-1}. All spectra were smoothed within the LabSolutionsIR software using a 10 point smoothing algorithm. The ATR crystal and pressure tip were cleaned and sterilized with

isopropyl alcohol in between each sample. A background spectrum was acquired before each powdered sample was placed on the ATR crystal and clamped down with the pressure tip. Each sample was run three times consecutively.

Lab standard minerals olivine, diopside, augite, anorthosite, calcite, dolomite, aragonite, montmorillonite, and kaolinite were also analyzed on the FTIR for comparison with the altered and unaltered samples.

Reference minerals, unaltered lava cave rocks, and HC samples 1 to 5, VAL samples 1 to 3, were plotted separately and stacked to identify key phases. Wavenumber regions that represent secondary minerals were identified within the altered samples by comparing the spectra of altered versus unaltered samples and identifying areas of interest within altered spectra that were not present or at different transmittance minima within unaltered spectra. Wavenumber regions corresponding to predicted secondary minerals were then compared against FTIR spectra of mineral standards and regions listed in the RRUFF database (Lafuente et al., 2015). Spectra of lab standard minerals and their associated RRUFF database profiles were also used to identify primary minerals within the spectra of unaltered samples.

Lyophilized biofilm samples from Golden Dome and Valentine caves were analyzed on the FTIR using the same settings as described for the rock and mineral samples.

2.3.4 Biology analysis

Swabs preserved in RNA later and lyophilized yellow biofilm scrapings were shipped to the Christopher Mason Lab at the Institute for Computational Biomedicine at Weill Cornell Medical College in New York, NY where DNA extractions were performed.

Whole genome sequencing was conducted by collaborators at the Mason Lab as part of the Extreme Microbiome Project (XMP) using the Oxford Nanopore Technologies PromitheION96. This long-read sequencing resulted in the creation of FASTQC/Krona plots to document phylum, class, genus, species, and biosynthetic gene clusters of the six biofilm cave samples collected at Lava Beds National Monument.

FINDINGS

3.1 Primary and Secondary Mineral Identification in Field Samples

Using both powder XRD and FTIR spectroscopy, the five secondary mineral coatings from samples collected within Hopkins Chocolate cave, three secondary mineral coatings from samples collected within Valentine cave, and one sample of unaltered wall rock collected from each respective cave were analyzed to determine their component minerals.

XRD data from the Hopkins Chocolate cave secondary mineral coating samples, shown in Figure 4A, show chlorite and kaolinite clay minerals at d-spacings of 7.14455 Å and 7.16284 Å within HC samples 1, 2, 3, and 4. HC sample 5, also shown in Figure 4A, shows the detection of prominent magnesite peaks at d-spacings of 2.73939 Å, 2.31494 Å, 2.09912 Å, and 1.94011 Å. All three Valentine Cave secondary mineral coatings, as in Figure 4B, show montmorillonite, kaolinite and nontronite clay minerals in addition to prominent calcite peaks at d-spacings of 3.86178 Å, 3.03535 Å, 2.84298 Å, 2.49438 Å, 2.28338 Å, and 2.09197 Å.

XRD data for Hopkins Chocolate and Valentine unaltered samples, shown in Figure 4C, confirm the presence of primary basalt-forming minerals such as pyroxene, olivine, and plagioclase. Diopside was used as the reference pyroxene family mineral while anorthite was used as the plagioclase family mineral for peak identification. The observed peaks on diffractograms corresponding to the unaltered cave rock are distinctly different from peaks which correspond to secondary minerals within HC samples 1 to 5 and VAL samples 1 to 3.

FTIR spectra from Hopkins Chocolate and Valentine Cave secondary mineral coatings, shown in Figures 5A and 5B, suggest kaolinite, nontronite, and montmorillonite. Kaolinite occurs in the HC and VAL coatings in the 800 cm^{-1} and 1000-1100 cm^{-1} wavenumber regions, while nontronite and montmorillonite appear in the 680 cm^{-1}, 900-1100 cm^{-1}, and 1650 cm^{-1} regions. Additionally, the presence of calcite is suggested in the VAL samples as shown in the 710 cm^{-1}, 880 cm^{-1} and 1425 cm^{-1} wavenumber regions. The wavenumber regions of kaolinite, montmorillonite, and calcite observed within the HC and VAL samples match those of related standard minerals shown in Figure 5D, and RRUFF database standards listed in Table 4.

FTIR spectra of the Hopkins Chocolate and Valentine unaltered samples, shown in Figure 5C, confirm XRD results and indicate pyroxene, olivine and plagioclase minerals. The wavenumber regions of these basalt-forming minerals observed within the HC and VAL unaltered samples match those of olivine, diopside, augite, and anorthosite standard minerals shown in Figure 5E as well RRUFF database standards listed in Table 4. The observed regions on the spectra corresponding to the unaltered cave rock are distinctly different from regions of interest which correspond to secondary minerals within HC samples 1 to 5 and VAL samples 1 to 3.

3.2 Biology

Three replicate biology samples were collected within each of the Golden Dome and Valentine Caves. Whole genome sequencing of biofilm samples collected from the walls of these two Lava Beds National Monument caves

showed phylum, class, genus, species, and biosynthetic gene clusters present in associated microbial communities.

Prominent phyla reported in both caves include actinomycetota, a gram-positive bacteria, and psuedomonadota, a gram-negative bacteria. Actinomycetota, also called actinobacteria, have been well documented in weathered volcanic rock deposits including other lava caves in Iceland, Canada, Hawaii, Portugal, Spain, and New Mexico (Cockell et al., 2013, Cheeptham, 2013, Riquelme et al., 2015). This phylum can be associated with the mobilization and solubilization of nutrients such as phosphates and iron, and can facilitate biological nitrogen fixation (Yadev et al., 2021).

Classes represented in high abundance include actinomycetes, alphaproteobacteria, betaproteobacteria, and gammaproteobacteria. Actinomycetia belong to the Actinomycetota phylum while alpha, beta, and gammaproteobacteria belong to the psuedomonadota phylum.

Genera from the Actinomycetota phylum include streptomyces, nocardia, mycobacterium, amycolatopsis and psuedonocardia, while pseudomonas, bradyrhizobium, and ruegeria represent genera from the psuedomonadota phylum.

Species observed in both caves include ruegeria pomeroyi, Psuedonocardia brossonetiae, Rhodococcus sp. 75, Pseudonocardia sp. DSM 110487, Pseudonocardia dioxanivorans and Pseudonocardia petroleophila. Additional species, Miltoncostaea marina, Miltoncostaea oceani and Rubrobacter marinus, were only documented in Valentine Cave.

Metabolic or biosynthetic gene clusters within species can produce secondary metabolites with unique functions. The most abundant biosynthetic gene clusters documented in both caves include lanthipeptide-class-i, terpene, NRPS, RRE-containing, RiPP-like, redox-cofactor, betalactone, and arylpolyene.

FASTQC/Krona plots, shown in Figure 6, display relative abundances of various phyla, classes, genera, species, and gene clusters present within the samples from the two caves.

FTIR spectra of lyophilized biofilm from Golden Dome and Valentine caves are shown in Figure 7. The spectra of these samples are similar to the montmorillonite lab standard mineral but contain an additional area of interest around 1550 cm^{-1} that possibly corresponds to the Amide II region.

3.3 Modeling products

Geochemical modeling results are summarized in Table 3 and reported as seven reaction progress steps with minerals at saturation or supersaturated listed for each step. These saturated minerals are considered plausible candidates for the secondary minerals observed within the selected cave sites at Lava Beds National Monument.

Eh values fall along the modeled reaction path. A changing Eh value is observed throughout the reaction with positive but decreasing values from 0.7428 to 0.5161 between steps 0 to 7 and negative and decreasing values from -0.3913 to -0.5239 between steps 12 to113. The remaining steps 113 to133 retain the same, negative Eh value of -0.5239. The negative Eh for later

xi steps and the equilibrated final value indicate reducing conditions are feasible.

pH values rise along the modeled reaction path. The pH increases throughout the reaction starting at 6.891 and reaching 10.868 by its conclusion. The increase in pH to the equilibrated final value >10 canonically indicates increased hydroxide availability; in a CO_2-rich atmosphere, some of this value is due to carbonate alkalinity also.

Minerals at saturation shift along the reaction path. In the initial stages of the reaction, clay (kaolinite, nontronite, saponite) and carbonate minerals (calcite) saturate in early reaction steps. Next, a new mineral assemblage emerges, characterized by the saturation of sulfide minerals (sphalerite, chalcopyrite, and pyrite). Calcite becomes undersaturated (reaction path step 24 (xi=0.0052) and is absent from subsequent model predictions. Later, sulfide and clay minerals are the primary minerals of interest. Gibbsite, prehnite, and Al oxyhydroxides may indicate the presence of additional Al-bearing clays; Al-phases saturate early and remain in model outputs until equilibrium is reached.

This model could be run at both a higher and lower temperature to assess differences in secondary mineral formation across a range of temperatures that represent expected environmental variations. At higher temperatures the reaction progress is expedited, while lower temperatures are expected to slow reaction progress.

DISCUSSION

4.1 Secondary Mineral Production in Weathering Basalts

Subaerial basalt weathering in oxidizing environments generates predictable secondary mineral assemblages, observed in diverse terrestrial settings, which form because of alteration processes such as silicification, carbonatization, chloritization, K-feldspar alteration, and albitization (Mathieu, 2018). Studies of alteration products from weathered flood basalt provinces document the presence of halloysite, montmorillonite, nontronite, and kaolinite in the Columbia River Basalt (Baker and Neill, 2017), while the Deccan volcanic province contains deposits of montmorillonite, hematite, ferruginous smectite, celadonite, and nontronite (Srivastava et al., 2018). Mafic rocks produced as a result of arc volcanoes in Oregon's Deschutes River Basin exhibit phosphate and smectite alteration products, with smectites primarily occurring because of plagioclase weathering and phosphates forming subsequently with small quantities of rare earth elements available in the same weathering solution that precipitated the clays (Frey et al., 2013). Icelandic basalts associated with rifting have shown to possess natrolite, analcime, chlorite, and calcite possibly formed from plagioclase minerals that have been corroded and chloritized over time (Viramonte et al., 1999, Kiselev et al., 2006, Tasaryova et al., 2018).

Key indicators of oxidizing environments include the carbonates, silicates (especially phyllosilicates), and sulfate minerals formed as secondary alteration or replacement products (Kettanah, 2019). Metal oxyhydroxide

formation is also feasible, including Fe-, Mn-, Cu-varieties, sometimes complexly mineralized with bound silica or carbonate components (e.g., chrysocolla, $Cu_2H_2Si_2O_5(OH)_4$ or malachite, $Cu_2 CO_3 (OH)_2$). Variations of these minerals are seen in diverse basalt weathering environments such as flood basalts, arc volcanoes, and rift basins, as summarized in table 5. Therefore, carbonate and clay minerals forming on basalt surfaces as modeled in this work are corroborated by other relevant low temperature basalt weathering studies and indicate the cave basalt's interaction with alteration fluids such as meteoric groundwater. The weathering of basalt through groundwater interactions can release cations such as $SiO_2(aq)$, Ca^{2+}, Na^+, and Mg^{2+}, which are later accounted for in secondary minerals like calcite, montmorillonite and magnesite as reported in this study and others concerning basalt cave weathering (Teehera et al., 2017).

Given the extremely active hydrologic cycle on Earth, secondary mineralogy is vulnerable to dissolution and tertiary alteration; thus, secondary minerals should be considered ephemeral. Hydrothermal alteration has the potential to further alter basalts that were previously weathered at low temperatures, often making it unclear whether the observed geochemical changes can be solely attributed to weathering (Wilson, 2004).

Lava cave environments have the potential to preserve minerals for a longer duration, in subsurface crevices and void spaces protected from physical/chemical weathering and erosion at the planetary surface. This may also be true for biofilms, which can survive for extended periods without water

if they are properly protected from prolonged radiation exposure (Billi et al., 2011, Baque et al., 2013, Billi, 2018, Billi et al., 2019, Mosca et al., 2019). Caves, in general, tend to have rich mineral content to facilitate geochemical reactions, and experience stable microclimates that produce perpetually dark, damp, low temperature and high CO_2 conditions, which are ideal in preserving residues of microbial activity and/or alteration products through time (Banerjee and Joshi, 2013, Çolak and Güngör, 2022). Studies from lava caves near the Hawaii-Space Exploration and Analog Simulation (HI-SEAS) document secondary minerals (e.g. gypsum, calcite, opal) that formed by hydrological interactions shortly after the formation and solidification of the caves and have been well preserved in the dry and isolated conditions ever since (Mulder et al., 2013).

The appropriateness of terrestrial basalts as Mars analogue environments has been well established with several sites on the island of Hawaii, Craters of the Moon National Monument in Idaho, and the San Carlos basalts in Arizona (Hadnott et al., 2017, Hughes et al., 2019). Additional lab-based studies have even exposed fresh basalt lithologies to aqueous solutions to estimate time intervals of clay formation on Martian basalts (Tangari et al., 2020). Specifically, the case for Lava Beds National Monument basalts as Mars analogue materials is strongly based on modal mineralogy consistent with known mafic meteorites from Mars and from spectral data collected on Mars surface rocks.

4.2 Lessons from FTIR/Candidate Organic-Mineral Associations in Mafic Rock Alteration

FTIR spectroscopy data of unaltered cave rocks and their associated secondary mineral samples underscore the mineral assemblage data from XRD findings and are summarized in table 6. Primary minerals observed in the unaltered cave rock XRD results, shown in figure 3C, include olivine, pyroxene, and plagioclase. These minerals are repeated in the FTIR spectra, shown in figure 4C, represented by the 550, 575 and 800-1100 cm^{-1} wavenumber regions as confirmed by lab standard primary mineral spectra shown in figure 4E. Similar regions that correspond to O-Si-O, Si-O, Si-O-Si, and Si-O stretching bonds are associated with olivine and pyroxene minerals (Choudhary et al., 2020), while O-Si(Al)-O bending, O-Si-O bending and Si (Al)-O stretching bonds are associated with plagioclase minerals (Matteson and Herron, 1993). Secondary cave minerals observed in both XRD and FTIR results, shown in figures 3A, B and 4A, B, include clays and carbonates. FTIR wavenumber regions of interest for clay minerals observed in the secondary deposits of both caves include 800, 950-1100, and 1650 cm^{-1} which match those of lab standard clays shown in figure 4D and correspond to the Si-O stretching, bending and OH bending bands in the 500-1300 cm^{-1} wavenumber regions (Madejová, 2003). Calcite, which was only observed in the spectra of secondary minerals from Valentine cave, are observed in the 710, 880, and 1350-1500 cm^{-1} wavenumber regions as confirmed by lab standard mineral spectra shown in figure 4D. These wavenumber regions correspond to the

symmetrical in-plane bend vibration mode of CO_3^{2-}, asymmetric out of plane vibration mode of CO_3^{2-}, and asymmetric stretching vibration mode of CO_3^{2-} respectively (Weir and Lippincott, 1961, Henry et al., 2017). Taken together, the FTIR spectra present expected signals based on the constituent bonds in the mixed mineral specimens.

The available carbon (+4 oxidation state) in carbonate groups/polyatomic ions can theoretically serve as a carbon resource for extreme cave life. Additionally, C can be sourced from CO_2 in the air or in dissolved organic matter such as acetate, organic acids, or humic acids that percolate through cave waters. The reduction of C in carbonate groups can be attributed to dissolved CO_2 (aq) coming into the cave via the overlying soil water at pH ~ 7 and speciating to HCO_3^- with lesser but significant CO_2 (aq), both compounds where O has a covalent double bond with C. Reviews of FTIR spectra of biofilm samples, summarized here and in table 7, highlight the wavenumber regions 1000 and lower, 1000-1132, 1272-1288, 1400, and 1637-1660 cm^{-1} as regions of interest to biological materials (Maquelin et al., 2002, Comte et al., 2006, Chen et al., 2013). Regions lower than 1000 cm^{-1} correspond to phosphate/sulfur functional groups while 1000-1132 cm^{-1} represent the C-O and C-C stretching, C-O-C and C-O-H deformation vibrations of polysaccharides structures. 1272-1288 cm^{-1} are amide III vibrations and 1400 cm^{-1} is the C=O symmetric stretching vibration of COO-. Lastly, 1637-1660 cm^{-1} acts as the signature for amide I vibration of proteins. Unfortunately, in natural samples such as in this study, all of these biologically-important

regions are associated with bonds within secondary minerals, though small inclusions of relict biological material could also be contained within the presented secondary cave minerals FTIR spectra, causing overlapping intensity dips or shoulders at the shared wavenumber regions.

Carbon present as dissolved organic carbon or extracellular polysaccharides (EPS) is generally lower in oxidation number–zero valent in sugars or most biomolecules. This is another carbon resource for diverse cave microbes, and in our own study locale 12 ± 8 mg/L of DOC were reported in the infiltrating cave waters (Kulkarni et al., 2022).

4.3 Comparison to Additional Studies and Other Lava Tube Sites

4.3.1 Mineralogy

Secondary minerals within lava caves in Hawaii, Idaho, Easter Island, and Iceland were compared to those detected in Lava Beds National Monument and are summarized in table 8. In Hawaii, Teehera et al. (2017) document the presence of calcite, gypsum, amorphous silica, and aluminum rich silicate minerals within two high altitude lava caves located on the northern flank of the Mauna Loa volcano. Secondary minerals within caves at Craters of the Moon National Monument in Idaho are dominated by Na-sulfates (henardite and mirabilite) with minor concentrations of Na-carbonates (trona and natron), carbonate-sulfate salt (burkeite) and calcium carbonate in the form of calcite and monohydrocalcite (Richardson et al., 2012). Easter Island's lava caves contain sepiolite (a magnesium silicate) and opal-A as the dominant secondary minerals, with additional detections of feldspar, calcite, and

smectite clays (Miller et al., 2014). Lastly, caves located within Icelandic lava fields contain the blue colored copper minerals chrysocolla and pseudomalachite, coupled with manganese oxide, carbonates, and an unnamed aluminum poor copper silicate (Kopacz et al., 2022). The presence of carbonate, sulfate, and smectite secondary minerals are widespread across diverse lava cave systems, though specific varieties are known to vary based on input water chemistry as seen with the enrichment of copper in the infiltrating cave waters described in Kopacz et al. (2022). This corroborates the findings from Lava Beds National Monument as carbonate and clay minerals are detected within the acquired secondary mineral samples and are likely heavily influenced by the associated ground waters described in Kulkarni et al. (2022).

4.3.2 Environmental microbiology

A review of the phyla of microbial life observed in diverse weathered volcanic rock deposits are summarized in table 8 and suggest Actinomycetota and Psuedomonadota (also known as actinobacteria and proteobacteria) are most prevalent in lava cave systems (Cockell et al., 2013, Riquelme et al., 2015, Lavoie et al., 2017, Teehera et al., 2017, Kopacz et al., 2022, Weng et al., 2022). Biofilm that was sampled for this work within the Golden Dome and Valentine caves also contained DNA consistent with the phyla Actinomycetota and Psuedomonadota and thus coincide with the extensive published lava tube microbiology literature. Species present in abundance in the sampled Lava Beds National Monument caves biofilm include Rhodococcus sp. 75 and

Ruegeria pomperoyi, along with several species belonging to the genus Pseudonocardia. Organisms from this genus were also present in cave and soil samples from Lava Beds National Monument analyzed by Lavoie et al. (2017). Biology samples collected within caves at Craters of the Moon National Monument contain organisms belonging to the order Psuedonocardiales (Weng et al., 2022), while caves within Icelandic lava fields vary slightly containing organisms belonging to the orders Burkholderiales (genus Ralstonia) and Caulobacter (genus Caulobacterales) (Kopacz et al. 2022). Groth et al. (2001) report on the ability of actinobacteria to induce the production of carbonate minerals such as calcite and vaterite by the species Rhodococcus. Given Rhodococcus' presence in the caves at Lava Beds National Monument, it is possible this species is using inorganic carbon as CO_2 to weather the basalt and precipitate carbonate mineral crystals (Groth et al. 2001, Cuezva et al., 2012).

Given the proximity of lava caves to the surface, the microbial communities within may be heavily influenced by organic carbon that leaches in through the overlying soil or water and provides a carbon source for cave life as described in various lava and karst cave studies (Poulson and Lavoie, 2001, Simon et al., 2003, 2007, Stegen et al., 2016, Miller et al., 2018). Examples of this are reported in Lavoie et al. (2017) where soil and cave organisms are compared to highlight similarities between bacterial communities on the surface and in the caves. Similarly, an analysis of cave water chemistry by Kulkarni et al. (2022) reports that the cave waters are enriched in plant-derived organic

matter acquired from the surface and are subsequently transported into the caves.

4.4 Support for Martian lava caves as environments with extremely strong preservation potential for life or associated minerals

Given Mars's distant past as a wet planet with a thicker Earth-like atmosphere (Fairén, 2010), it is possible that aqueous alteration of Martian basalt precipitated secondary minerals such as carbonates and clays, as observed in terrestrial settings (Gislason et al., 1992, Leveille et al., 2002, Teehera et al., 2017). Calcium carbonate minerals are sparsely observed in ground and satellite-based spectrometer readings of the whole Martian surface, though have been observed near clay minerals in isolated areas such as the Nilli Fossae (Ehlmann et al., 2008), Gusev Crater (Morris et al., 2010), the Phoenix lander site (Boynton et al., 2009) and in Martian meteorites (Niles et al., 2012) indicating the alteration of olivine by surface water or hydrothermal fluids. Though deposits are isolated on the surface, they may be widespread throughout shallow lava caves where they formation via interactions with the once thick CO2-rich atmosphere and have been preserved ever since (Mulder et al., 2023). The presence of these minerals within lava caves would subsequently indicate percolation of groundwater in the Martian subsurface and may have allowed for microorganisms, similar to those seen in terrestrial lava caves, to exist within these humid sheltered environments.

The accumulation of stable deposits of water ice has been proposed in present day Martian lava caves by modeling results (Williams et al., 2010). Ice or associated thin films of liquid water housed within sheltered Martian lava cave environments and exposed to basalt rock, may be viable locations for the formation of simple life. Ice associated microbes have been observed within Hawaiian lava caves (Teehera et al., 2017) and a study by Popa et al., (2012) has shown basalt-ice interface microbes in terrestrial lava caves can metabolize iron from olivine. If Martian lava caves were exposed to liquid water or ice in the past or present, it is possible that chemolithoautotrophic species similar to the actinobacteria or proteobacteria widely associated with terrestrial lava caves, including those at Lava Beds National Monument, may be present and contributing to the precipitation of carbonate minerals.

4.5 Future Directions

The basalt-water reaction model described herein is relevant for terrestrial lava cave environments. Additional studies could modify the existing geochemical model to represent Mars conditions by altering the temperature, atmospheric pressure, mineral inputs, and aqueous solution chemistry. The temperature of the reaction could be run at both near zero and 20 degrees C to simulate diverse Martian surface conditions, while atmospheric pressure could be decreased. Mineral inputs, which determine rock chemistry, could be altered to better mimic known Martian basalts/meteorites. Aqueous solution model inputs could be altered to match speculated Mars fluid compositions consisting of perchlorate-type water with high salinity levels (Chevrier et al.,

2022). Secondary minerals produced in the Mars simulant models could then be compared to the terrestrial model outputs to determine differences in alteration products.

CONCLUSIONS

- The formation of carbonate and clays as secondary minerals in lava caves can be detected and differentiated from the primary mineral composition of the host rock using spectroscopic techniques.
- Observed secondary minerals are the reaction products of the basalt rock chemistry interacting with meteoric groundwater compositions and are predicted by geochemical models as forming in the initial stages of the reaction.
- The presence of carbonate and clay minerals indicates the water-rock reactions within lava caves at Lava Beds National Monument are ongoing and have not yet reached thermodynamic equilibrium.
- Disequilibrium can drive energic reactions amongst cave dwelling microbes, which in turn, may contribute to the production of secondary minerals.

TABLES

Table 1: Lava Beds National Monument estimate of modal mineral compositions adapted from Hart et al. (1984), as mineral inputs to the geochemical model.

Mineral	Modal Quantity (kg)
Forsterite	0.18
Fayalite	0.06
Diopside	0.20
Enstatite	0.03
Anorthite	0.47
Magnetite	0.06

Table 2: Lava Beds National Monument estimate of cave water chemistry composed of major elements, anions, and trace elements used in the geochemical model. Adapted from Kulkarni et al. (2022).

Component	Quantity
H2O	1.0 free kg
Na+	8.0 mg/l
Cl-	4.0 mg/l
Fe++	2.0 mg/l
Mg++	4.0 mg/l
Ca++	4.0 mg/l
Al+++	2.0 mg/l
SiO2 (aq)	22.0 mg/l
H+	7.0 (pH)
HCO3-	35.0 mg/l
SO4--	2.0 mg/l
NO3-	9.0 mg/l
Sr++	50.0 ug/l
Cu+	50.0 ug/l
Zn++	50.0 ug/l
V+++	10.0 ug/l
Cr+++	10.0 ug/l
Mn++	10.0 ug/l
O2 (aq)	10.0 ug/l

Table 3: Select reaction progress steps and their associated minerals at saturation, Eh, and pH values. Blue = clay minerals, yellow = carbonate minerals, red = sulfide minerals, and * = Al-rich minerals potentially substituting for Al-rich clays.

Reaction Progress	Eh (volts)	pH	Minerals at Saturation
Xi = 0 Step = 0	+0.7428	6.891	Nontronit-Mg Quartz Kaolinite Pyrolusite
Xi = 0.0001 Step = 2	+0.6175	8.694	Kaolinite Nontronit-Ca Saponite-Ca Dolomite-ord Dolomite Pyrolusite Tenorite Gibbsite* Strontianite
Xi = 0.0003 Step = 7	+0.5161	10.123	Pyrolusite Tenorite Ferrite-Zn Calcite Gibbsite* Strontianite Andradite Nontronit-Ca Saponite-Ca Prehnite
Xi = 0.0009 Step = 12	-0.3913	10.182	Calcite Saponite-Ca ZnCr2O4 Gibbsite* Nontronit-Ca Strontianite Sphalerite Andradite Prehnite Pyrite Chalcopyrite
Xi = 0.5000 Step = 83	-0.5238	10.866	Ripidolit-14A Clinochl-14A Sphalerite ZnCr2O4 Gibbsite* Saponite-Ca Andradite Chalcopyrite Pyrite Prehnite
Xi = 0.8000 Step = 113	-0.5239	10.867	Ripidolit-14A Clinochl-14A Sphalerite ZnCr2O4 Gibbsite* Saponite-Ca Andradite Chalcopyrite Pyrite Prehnite
Xi = 1.0000 Step = 133	-0.5239	10.868	Ripidolit-14A Clinochl-14A Sphalerite ZnCr2O4 Gibbsite* Saponite-Ca Andradite Chalcopyrite Pyrite Prehnite

Table 4: FTIR regions of primary and secondary minerals from lab standards and published RRUFF database reference standards.

Mineral	FTIR Region of Interest - Lab Standards	FTIR Region of Interest - Reference Standards
Olivine	800-1100	800-1100 (individual peaks/shoulders 1000, 900, 870)
Diopside	800-1100	800-1100 (individual peaks/shoulders 1080, 990, 860)
Augite	800-1100	800-1100 (individual peaks/shoulders 1080, 980, 875)
Anorthosite	540, 575, 700-800, 800-1100	525, 575, 730, 750, 900, shoulders 1000, 1090, 1210
Calcite	710, 880, 1400, 1800	710, 875, 1400, 1800
Magnesite		750, 880, 1400
Montmorillonite	900-1100, 1650	
Kaolinite	680, 1000-1200	
Nontronite		600, 675, 900-1100, 1650

Table 5: Summary of secondary minerals observed in diverse subaerial weathered basalt settings.

Location	Secondary Minerals	Formula	References
Flood Basalt Provinces	Halloysite + Montmorillonite + ✧ Nontronite + ✧ Hematite ✧ Kaolinite + Ferruginous smectite ✧ Celadonite ✧	$Al_2Si_2O_5(OH)_4 \cdot nH_2O$ $(Na,Ca)_{.33}(Al,Mg)_2(Si_4O_{10})(OH)_2 \cdot nH_2O$ $Ca_{.5}(Si_7Al_{.8}Fe_{.2})(Fe_{3.5}Al_{.4}Mg_{.1})O_{20}(OH)_4$ Fe_2O_3 $Al_2Si_2O_5(OH)_4$ $K(Mg,Fe^{2+})(Fe^{3+},Al)(Si_4O_{10})\ (OH)_2$	Baker and Neill (2017) + Srivastava et al. (2018) ✧
Mafic Rocks Produced by Arc Volcanoes	Iddingsite Allophane Halloysite Kaolinite Iron oxide-hydroxides	$MgO \cdot Fe_2O_3 \cdot 3SiO_2 \cdot 4H_2O$ $Al_2O_3 \cdot (SiO_2)_{1.3\text{-}2} \cdot (2.5\text{-}3)H_2O$ $Al_2Si_2O_5(OH)_4 \cdot nH_2O$ $Al_2Si_2O_5(OH)_4$	Frey et al. (2013)
Rift Basalts	Natrolite ¤ Analcime ¤ Calcite ★ ¤ ◎ Chlorite ◎	$Na_2Al_2Si_3O_{10} \cdot 2H_2O$ $NaAlSi_2O_6 \cdot H_2O$ $CaCO_3$ $(Mg,Fe)_3(Si,Al)_4O_{10}(OH)_2 \cdot (Mg,Fe)_3(OH)_6$	Viramonte et al. (1999) ¤ Tasaryova et al. (2018) ★ Kiselev et al. (2006) ◎

Table 6: Summary of FTIR wavenumber regions of interest for primary basalt forming minerals and their associated secondary minerals.

Mineral	Wavenumber Region cm^{-1}	Bond Description	Reference
Primary Minerals			
Olivine	800-1100	O-Si-O, Si-O, Si-O-Si, and Si-O stretching bonds	Choudhary et al. (2020)
Pyroxene			
Plagioclase	540, 575, 700-800, 800-1100	O-Si(Al)-O bending, O-Si-O bending and Si (Al)-O stretching bonds	Matteson and Herron (1993)
Secondary Minerals			
Clays	800, 950-1100, and 1650	Stretching, bending and OH bending bands	Madejová (2003)
Carbonates	710, 880, and 1350-1500	Symmetrical in-plane bend vibration mode of CO_3^{2-}, asymmetric out of plane vibration mode of CO_3^{2-}, and asymmetric stretching vibration mode of CO_3^{2-}	Weir and Lippincott (1961) Henry et al. (2017)

Table 7: Summary of FTIR wavenumber regions of interest for biological materials that may be present in secondary mineral or biofilm samples.

Biological Material	Wavenumber Region cm^{-1}	Indicative Meaning	Reference
Phosphate/sulfur functional groups	1000 and lower	Backbone of DNA, amino acids	Maquelin et al. (2002) Comte et al. (2006) Chen et al. (2013) Bruggemann et al. (2023)
C-O and C-C stretching, C-O-C and C-O-H deformation vibrations of polysaccharides structures	1000-1132	Extracellular polymeric substance (EPS)	
Amide III vibrations	1272-1288	Proteins (peptidic bond) N–H in-plane bending and C–N stretching vibration	
C=O symmetric stretching vibration of COO-	1400	Amino acid and carboxylic acid	
Amide II	1520-1550	NH_2 deformation, N-H bending and C-N stretching in secondary amides	
Amide I vibration of proteins	1637-1660	Proteins (peptidic bond) C–N and C=O stretching vibration	

Table 8: Summary of secondary minerals and organic materials present in diverse lava cave locations. Data pertaining to Lava Beds National Monument is highlighted in yellow.

Location	Minerals	Formula	Organics	Reference
Mauna Loa, Hawaii, USA	Calcite Gypsum Amorphous silica	$CaCO_3$ $CaSO_4 \cdot 2\ H_2O$ SiO_2	Phyla: Actinobacteria Proteobacteria	Teehera et al. (2018)
Craters of the Moon, Idaho, USA	Thenardite Mirabilite Trona Natron Burkeite Calcite Monohydrocalcite	Na_2SO_4 $Na_2SO_4 \cdot 10H_2O$ $Na_3H(CO_3)_2 \cdot 2H_2O$ $Na_2CO_3 \cdot 10H_2O$ $Na_4(SO_4)(CO_3)$ $CaCO_3$ $CaCO_3 \cdot H_2O$	Phylum: Actinobacteria Order: Pseudonocardiales	Richardson et al. (2012) Weng et al. (2022)
Ana Heva lava tube Easter Island, Chile	Sepiolite Opal-A Feldspar Calcite Smectite clays	$Mg_4Si_6O_{15}(OH)_2 \cdot 6H_2O$ $SiO_2 \cdot nH_2O$ $CaCO_3$	Phylum: Actinobacteria	Miller et al. (2014)
Southern Eldhraun lava field and northern Ódáðahraun lava field, Iceland	Chrysocolla Pseudomalachite Manganese oxide Carbonates Aluminum poor copper silicate	$Cu_2H_2Si_2O_5(OH)_4$ $Cu_5(PO_4)_2(OH)_4$ MnO_2	Phylum: Proteobacteria Order: Burkholderiales, Caulobacter	Kopacz et al. (2022)
Lava Beds National Monument, CA, USA	Calcite Magnesite Montmorillonite Nontronite Kaolinite Chlorite	$CaCO_3$ $MgCO_3$ $(Na,Ca)_{.33}(Al,Mg)_2(Si_4O_{10})(OH)_2 \cdot nH_2O$ $Ca_{.5}(Si_7Al_{.8}Fe_{.2})(Fe_{3.5}Al_{.4}Mg_{.1})O_{20}(OH)_4$ $Al_2Si_2O_5(OH)_4$ $(Mg,Fe)_3(Si,Al)_4O_{10}(OH)_2 \cdot (Mg,Fe)_3(OH)_6$	Phyla: Actinobacteria Proteobacteria Order: Pseudonocardiales	Lavoie et al. (2017)

FIGURES

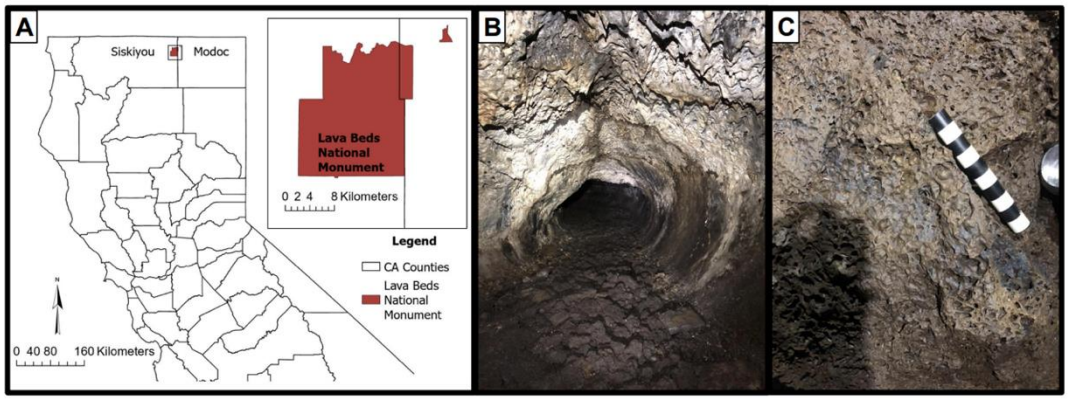

Figure 1: **A)** shows the general study area, Lava Beds National Monument, highlighted in red. **B)** shows an example of a lava cave located within Lava

Beds National Monument. This cave is approximately 1 meter in height and exhibits an a'a textured lava flow on its floor. **C)** shows the texture of the basalt cave wall rock with 10 cm bar for scale.

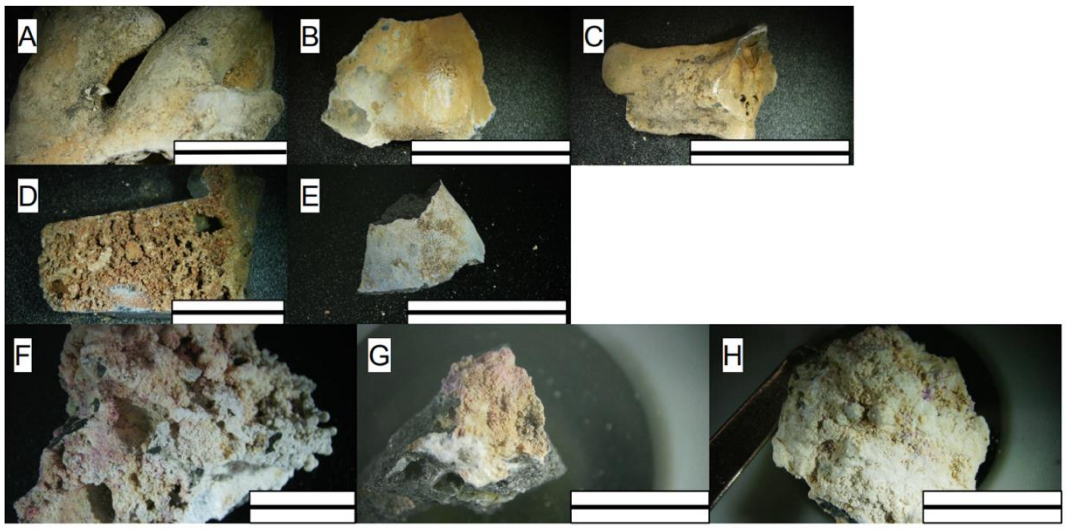

Figure 2: Photos of altered samples show secondary mineral samples collected in Hopkins Chocolate and Valentine caves. A-E correspond to HC samples 1 through 5. F-H correspond to VAL samples 1 through 3. All scale bars are 1 cm in length.

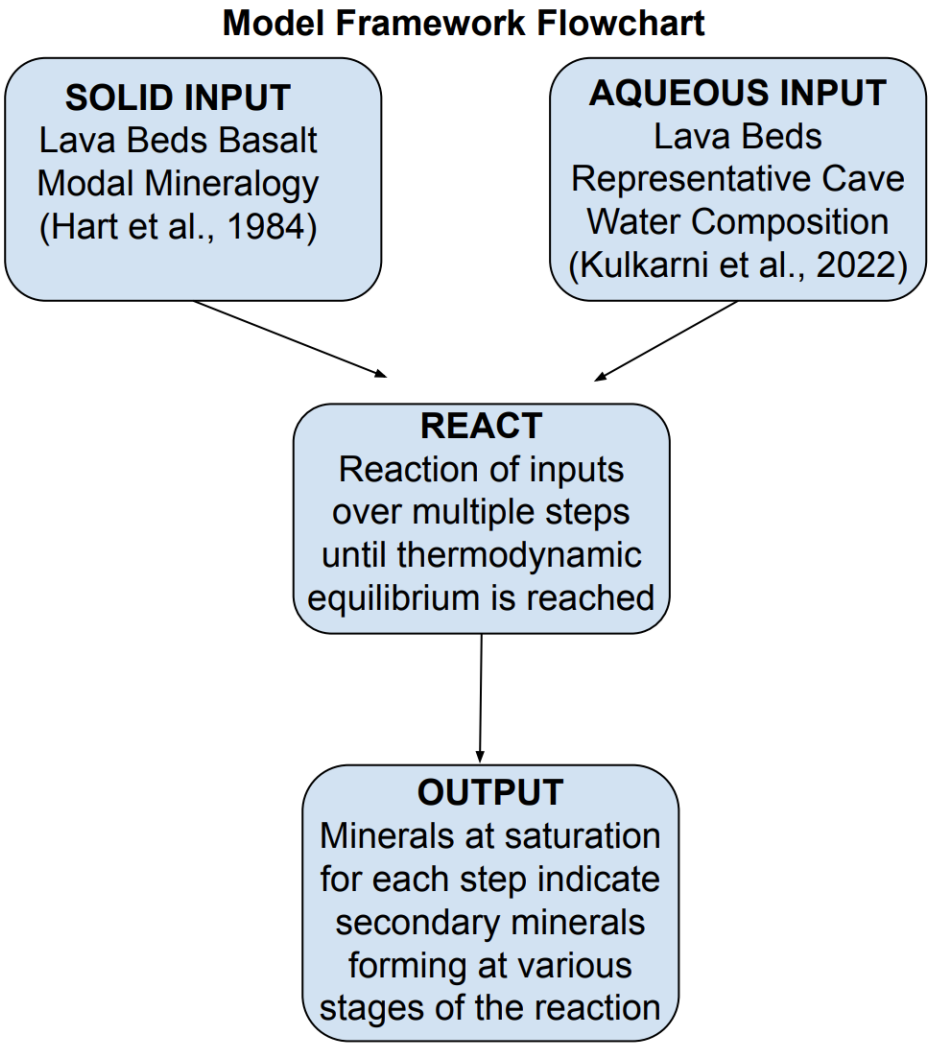

Figure 3: Model framework flowchart describing the geochemical model inputs and outputs.

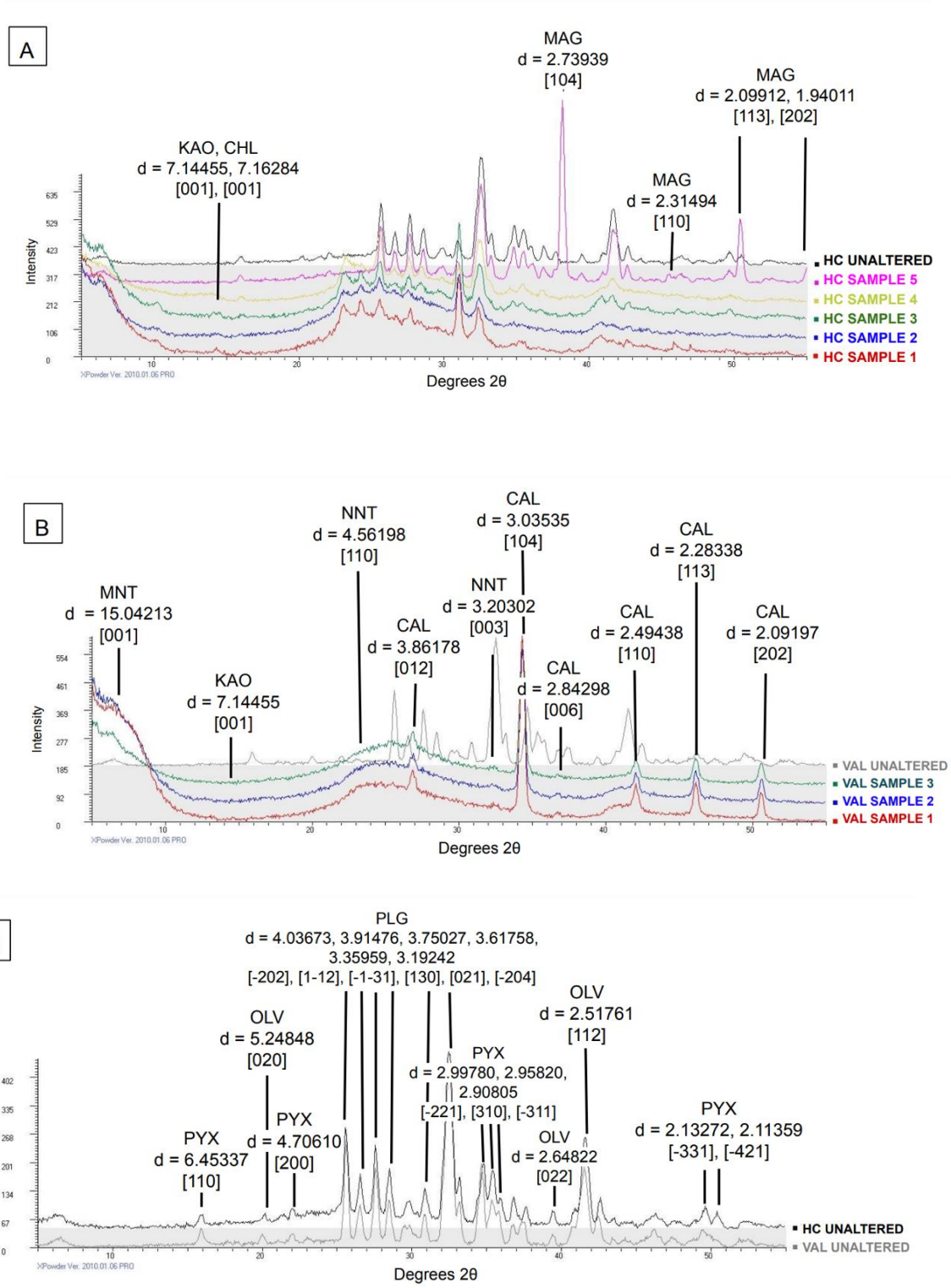

Figure 4: **A)** X-ray diffractograms of unaltered basalt and secondary mineral samples from Hopkins Chocolate cave. Mineral abbreviations, d spacings and miller indices correspond to secondary minerals identified within HC samples

1-5. **B)** X-ray diffractograms of unaltered basalt and secondary mineral samples from Valentine cave. Mineral abbreviations, d spacings and miller indices correspond to secondary minerals identified within VAL samples 1-3. **C)** X-ray diffractograms of unaltered basalt samples collected from cave walls within Hopkins Chocolate and Valentine caves. Mineral abbreviations, d spacings and miller indices correspond to primary minerals identified within the HC and VAL unaltered samples.

PYX = Pyroxene, OLV = Olivine, PLG = Plagioclase, MNT = Montmorillonite, NNT = Nontronite, KAO = Kaolinite, CHL = Chlorite, MAG = Magnesite, and CAL = Calcite.

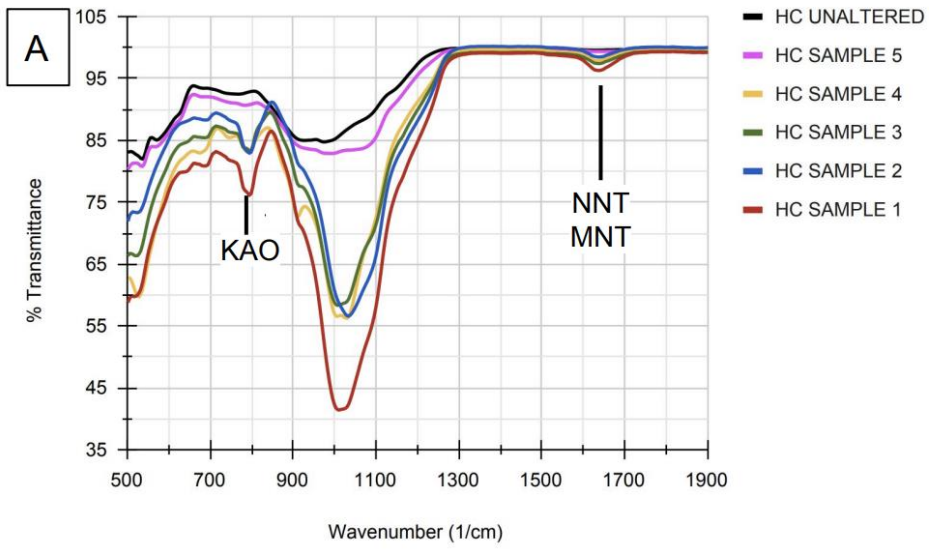

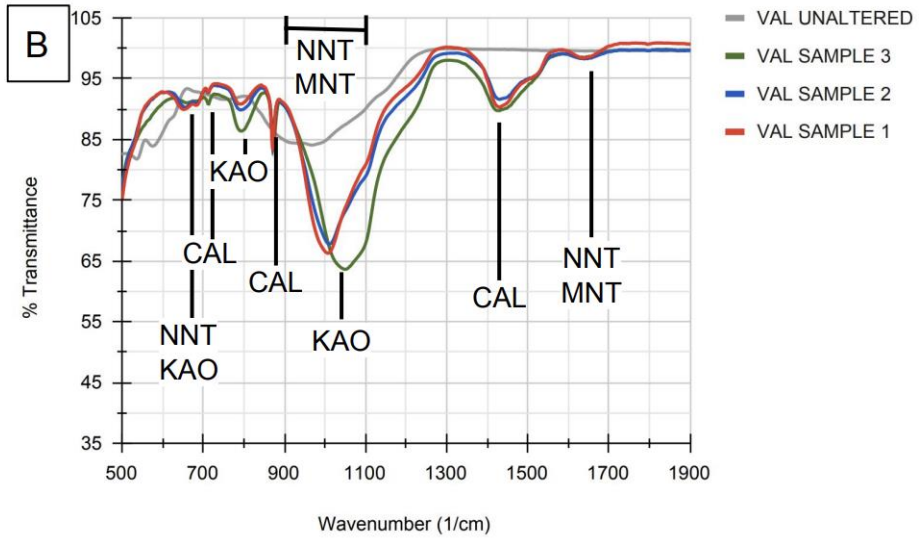
B
VAL UNALTERED
VAL SAMPLE 3
VAL SAMPLE 2
VAL SAMPLE 1
% Transmittance
Wavenumber (1/cm)
NNT
MNT
KAO
CAL
CAL
NNT
KAO
KAO
CAL
NNT
MNT

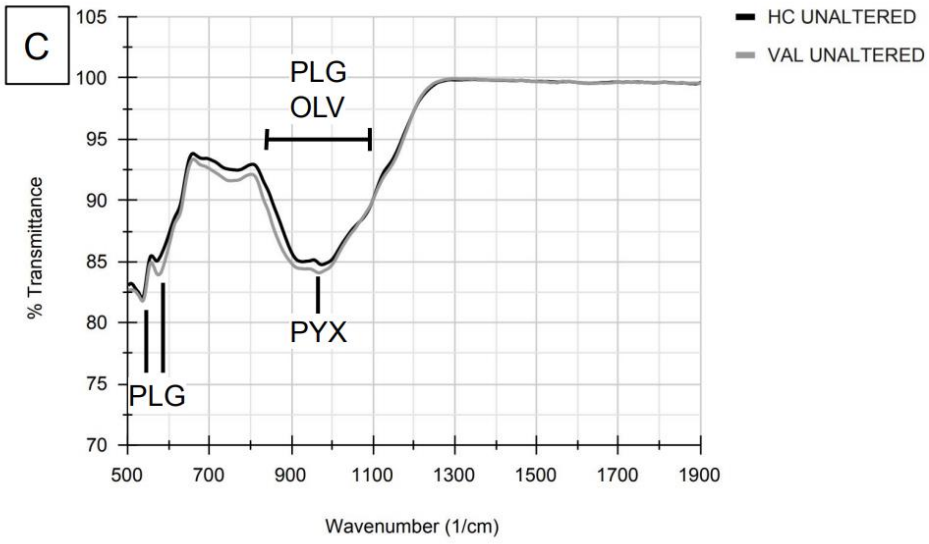
C
HC UNALTERED
VAL UNALTERED
% Transmittance
Wavenumber (1/cm)
PLG
OLV
PYX
PLG

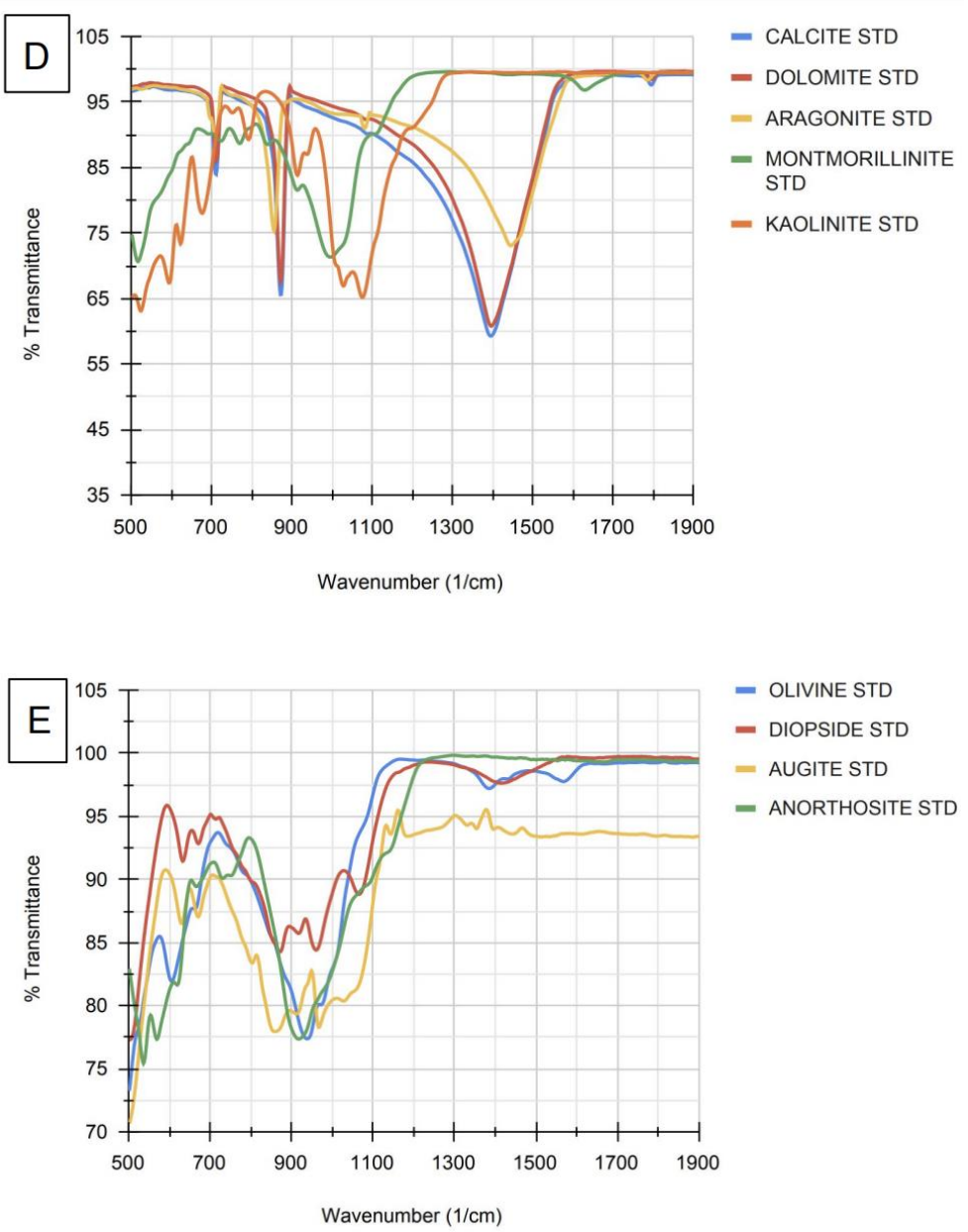

Figure 5: **A)** FTIR spectra of unaltered basalt and secondary mineral samples from Hopkins Chocolate cave. Mineral abbreviations correspond to secondary minerals identified within HC samples 1-5. **B)** FTIR spectra of unaltered basalt and secondary mineral samples from Valentine cave. Mineral abbreviations correspond to secondary minerals identified within VAL samples 1-3. **C)** FTIR spectra of unaltered basalt samples collected from cave walls within Hopkins

Chocolate and Valentine caves. Mineral abbreviations correspond to primary minerals identified within the HC and VAL unaltered samples.

PYX = Pyroxene, OLV = Olivine, PLG = Plagioclase, MNT = Montmorillonite, NNT = Nontronite, KAO = Kaolinite, and CAL = Calcite.

D) FTIR spectra of lab standard secondary minerals. **E)** FTIR spectra of lab standard primary minerals.

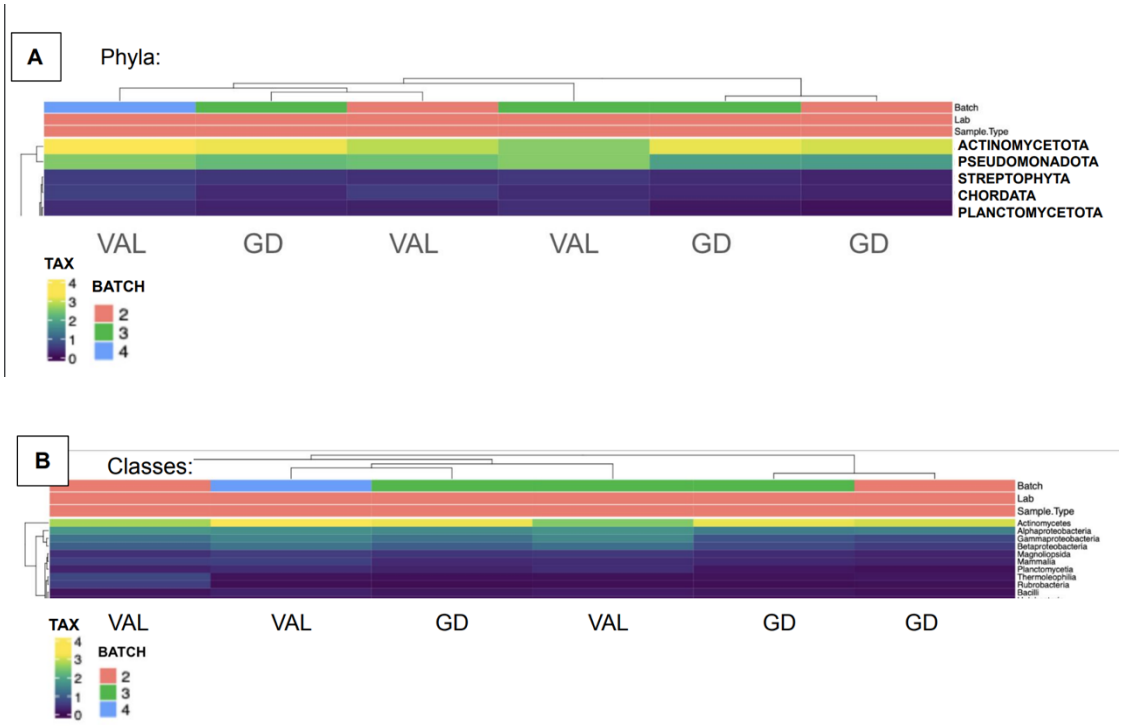

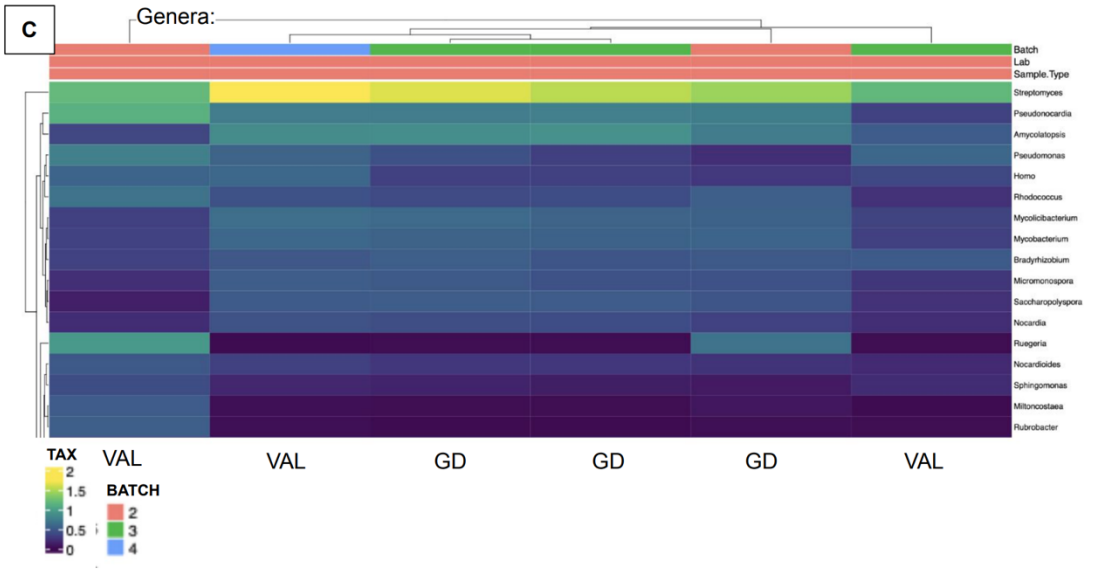
C
Genera:
Batch
Lab
Sample.Type
Streptomyces
Pseudonocardia
Amycolatopsis
Pseudomonas
Homo
Rhodococcus
Mycolicibacterium
Mycobacterium
Bradyrhizobium
Micromonospora
Saccharopolyspora
Nocardia
Ruegeria
Nocardioides
Sphingomonas
Miltoncostaea
Rubrobacter
VAL
VAL
GD
GD
GD
VAL
TAX
2
1.5
1
0.5
0
BATCH
2
3
4

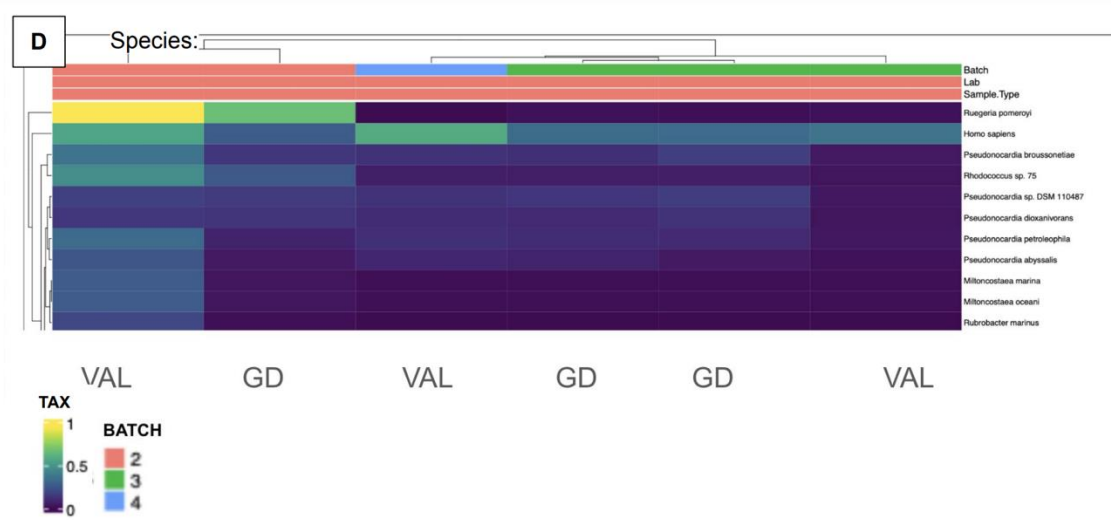
D
Species:
Batch
Lab
Sample.Type
Ruegeria pomeroyi
Homo sapiens
Pseudonocardia broussonetiae
Rhodococcus sp. 75
Pseudonocardia sp. DSM 110487
Pseudonocardia dioxanivorans
Pseudonocardia petroleophila
Pseudonocardia abyssalis
Miltoncostaea marina
Miltoncostaea oceani
Rubrobacter marinus
VAL
GD
VAL
GD
GD
VAL
TAX
1
0.5
0
BATCH
2
3
4

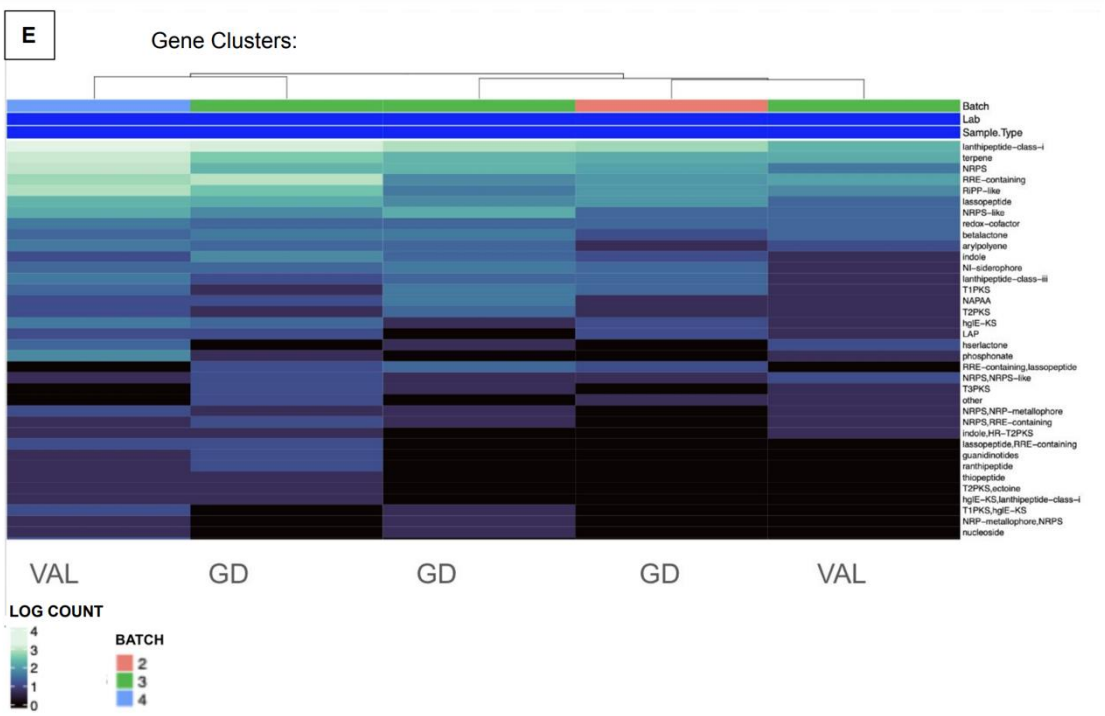

Figure 6: FASTQC/Krona plots of biology samples collected within Golden Dome And Valentine caves. **A)** Shows phyla **B)** shows classes **C)** shows genera **D)** shows species **E)** shows gene clusters. Bright colors indicate higher abundance while dark colors indicate low abundance. GD = Golden Dome and VAL = Valentine

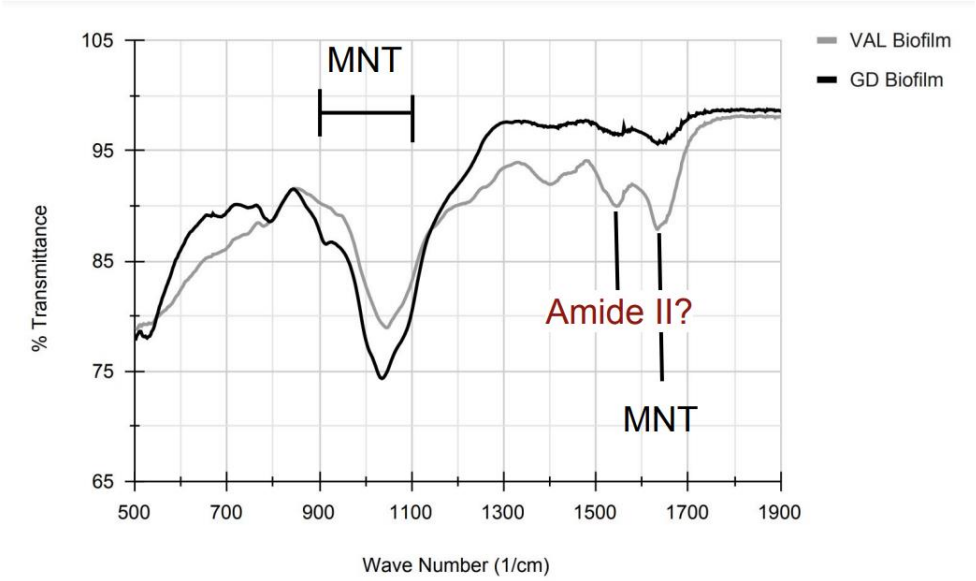

Figure 7: FTIR spectra of lyophilized biofilm collected within Golden Dome and Valentine caves. Wavenumber regions corresponding to montmorillonite are labeled as MNT, while the wavenumber region potentially associated with Amide II is labeled in red.

APPENDICES

Appendix A: XRD data from additional secondary mineral samples.

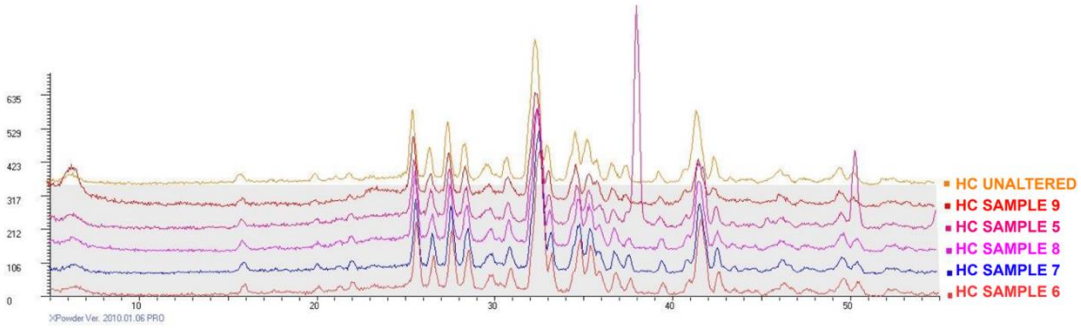

Figure 1: X-ray diffractograms for five Hopkins Chocolate cave surface samples, one HC unaltered diffractogram is shown stacked against four altered sample diffractograms (HC samples 5-9). HC sample 5 was featured in this work while HC samples 6, 7, 8, and 9 were not.

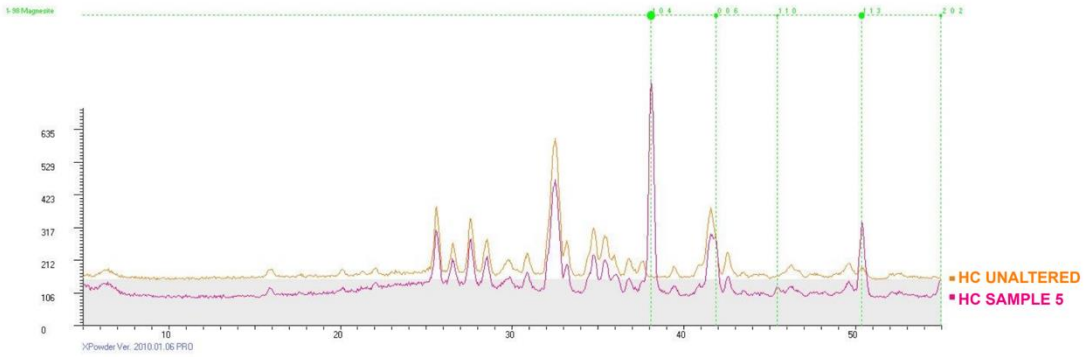

Figure 2: Diffractograms of HC unaltered and HC sample 5 are isolated to highlight peak locations. Peak identifying software, XPowder, shows peaks corresponding to the mineral magnesite in HC sample 5.

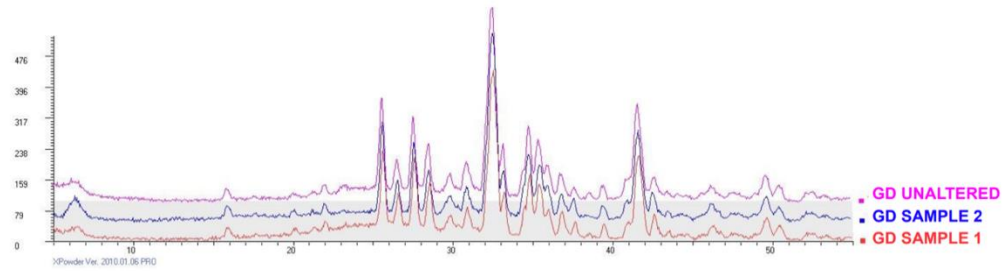

Figure 3: Stacked X ray diffractograms of unaltered wall rock and two secondary mineral samples collected from the Golden Dome cave at Lava Beds National Monument.

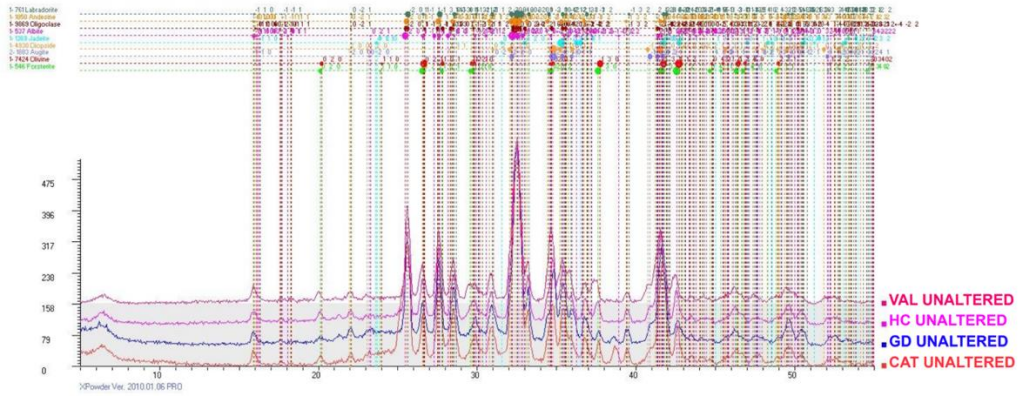

Figure 4: Stacked X-ray diffractograms of unaltered cave wall rock from the four sampled caves (Valentine, Hopkins Chocolate, Golden Dome, and Catacombs). Potential basalt forming component minerals are shown above.

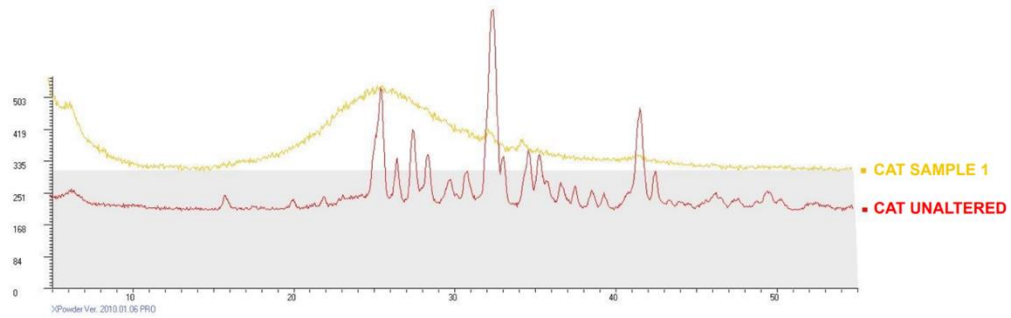

Figure 5: Stacked X ray diffractograms of unaltered wall rock and one secondary mineral sample collected from the Catacombs cave at Lava Beds National Monument. CAT sample 1 is amorphous and exhibits no distinct crystalline mineral peaks.

Appendix B: FTIR data from additional secondary mineral samples.

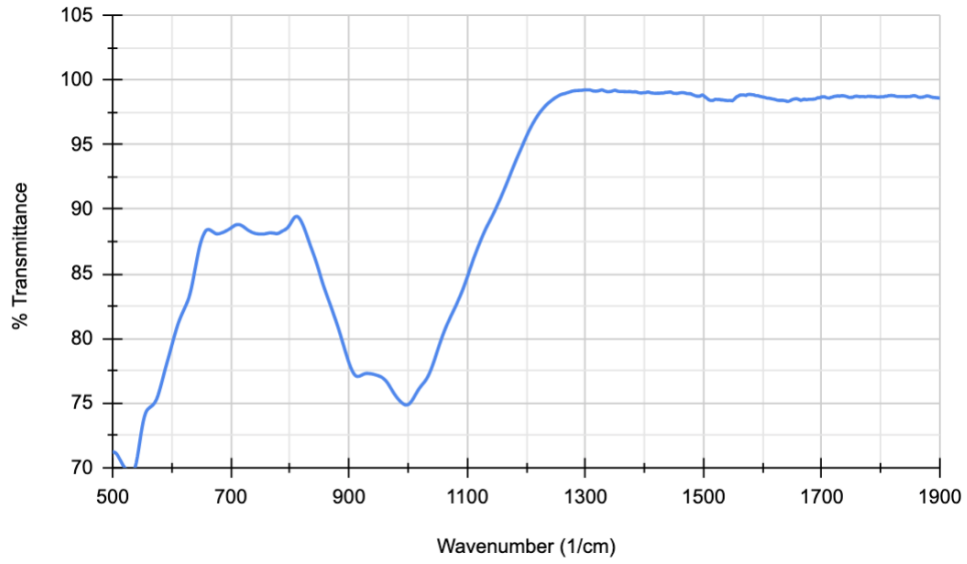

Figure 1: FTIR spectra of Catacombs unaltered cave rock.

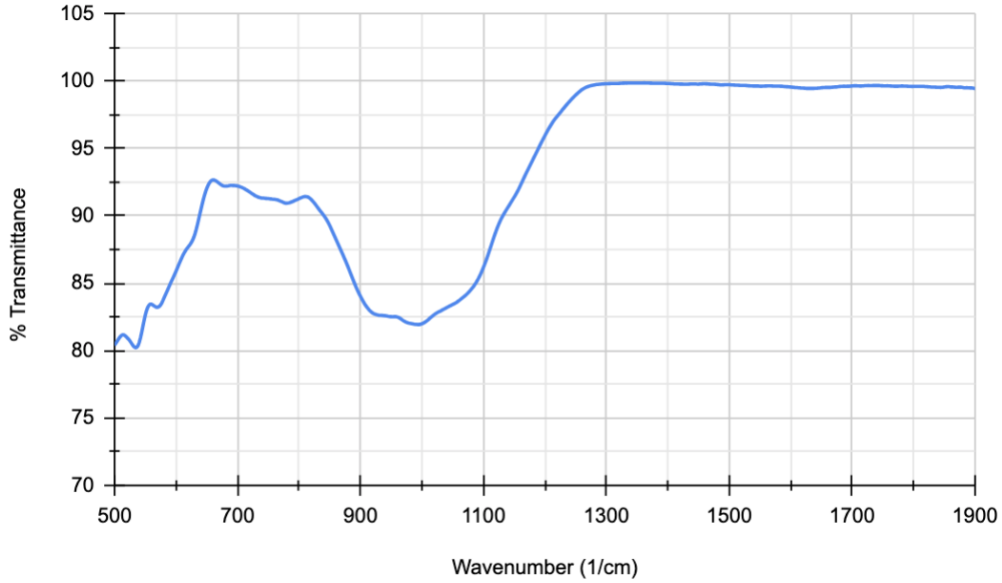

Figure 2: FTIR spectra of CAT sample 1, a secondary mineral sample collected within Catacombs cave.

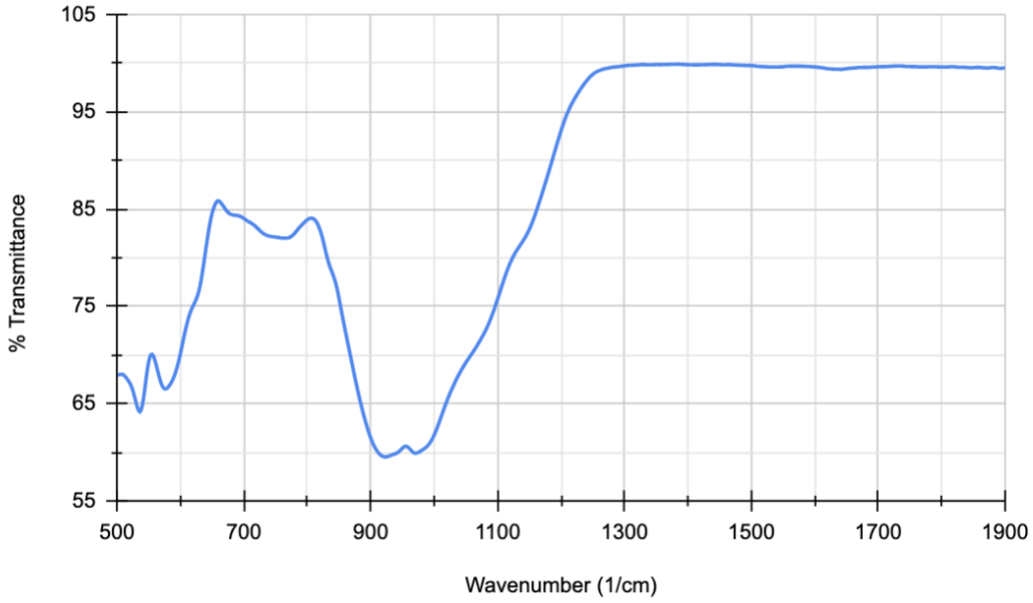

Figure 3: FTIR spectra of GD sample 1, a secondary mineral sample collected within Golden Dome cave.

Table 1: Binned FTIR wavenumber regions (from 499-1999 cm^{-1}) and associated % transmission values of additional unaltered and altered samples from Hopkins Chocolate, Catacombs, Valentine, and Golden Dome Caves.

%Transmittance mean of cave samples

Wavele	HC-LAB	HC-1A	HC-1B	HC-1C	HC-1D	HC-1E	HC-RED	CAT-LAB	CAT-1A	CAT-1B	VAL-LAB	VAL-1A	VAL-PIN	GD-LAB	GD-1A	GD-BLUE
499-549	82.86722	66.46334	79.11675	84.672	71.85575	79.73269	56.92927	70.91893	80.90258	86.67962	82.49643	83.31906	80.32009	75.92237	81.79182	78.18669
549-599	82.86197	73.13311	82.19278	87.34986	77.92882	83.23393	69.13439	76.23387	83.94646	89.8777	84.62697	85.49278	87.82056	80.14533	84.6875	81.46689
599-649	85.66493	81.23734	86.98834	90.77109	84.46574	87.69976	77.36026	83.08087	88.29165	92.36609	88.87849	89.01593	88.51463	85.7122	88.74412	86.47092
649-699	89.64608	84.50035	91.61293	93.8651	88.20247	91.59537	79.80403	88.43688	92.32631	93.11569	92.96557	91.36145	87.91246	90.6605	92.61081	91.44342
699-749	93.54879	88.42451	90.77535	93.4576	88.61099	91.04586	83.96993	88.72421	91.69514	93.0073	92.0826	91.20638	90.49101	90.18091	91.94675	90.60519
749-799	92.91653	92.13814	90.15056	93.13722	87.7702	90.39633	83.28978	88.47359	91.11746	90.77786	91.77808	91.76923	89.13772	89.75379	91.23298	90.21132
799-849	92.59873	91.58159	89.48564	92.85196	87.82029	90.1746	84.19152	88.28465	90.77025	91.7632	90.78297	91.58395	89.97895	88.92642	90.8285	89.46528
849-899	91.97772	90.85968	84.70985	90.04978	83.24739	86.14288	77.11922	82.10813	86.80316	93.33002	86.45708	87.49245	88.91433	83.33853	87.0734	84.03806
899-949	87.98396	90.59197	80.8985	87.70406	78.05309	82.01092	71.14203	77.60314	82.94064	89.69947	84.49638	84.5573	84.95013	79.07132	83.31296	80.15183
949-999	85.13793	87.2702	80.52854	87.21503	74.83047	80.76759	63.00004	76.24008	82.19677	85.88388	84.28751	84.52724	71.46589	78.65616	82.74414	79.91733
999-1049	84.93664	83.93554	81.66573	87.36633	71.77935	80.98264	59.36538	76.84073	82.72933	77.10558	86.11271	85.93488	68.32672	80.06429	82.98094	82.18855
1049-1099	86.46193	83.07786	83.61123	88.51657	76.16496	82.85624	73.91752	82.13837	84.41609	73.9491	88.61435	88.6882	75.25224	83.30318	83.84565	84.78193
1099-1149	88.66033	83.28631	88.32321	91.6515	84.51842	87.87695	84.69168	87.86472	89.03391	82.5051	91.71033	91.86985	83.31108	88.69062	88.42086	89.33136
1149-1199	92.06726	84.06866	93.10805	95.01097	91.11715	92.79709	91.88725	93.106	93.61033	89.1888	95.10604	95.2654	89.74657	93.54069	93.28372	93.76442
1199-1249	95.40358	88.78171	97.38173	97.89812	95.77683	96.95254	95.35599	97.63514	97.58122	93.17249	98.69429	98.64634	93.37757	97.90978	97.33794	98.09083
1249-1299	98.63118	93.36965	99.33879	99.27675	99.11895	99.15389	98.54289	99.23534	99.51695	98.07205	99.81848	99.83566	97.71191	99.7029	99.53553	99.59216
1299-1349	99.74749	97.12949	99.66309	99.49544	99.82967	99.5488	99.2603	99.40633	99.82641	99.31585	99.92829	99.95142	98.59785	99.95933	99.9318	99.7928
1349-1399	99.86777	99.33515	99.66538	99.47908	99.83544	99.55567	99.21815	99.32172	99.84023	99.3987	99.86609	99.91503	97.36683	99.93021	99.94324	99.77413
1399-1449	99.84755	99.75244	99.61501	99.44091	99.79971	99.49682	99.15162	99.24492	99.77995	99.27633	99.82676	99.87935	92.73706	99.87413	99.89991	99.7296
1449-1499	99.80275	99.7465	99.5618	99.39613	99.73576	99.43121	99.12529	99.15401	99.75358	99.262	99.77589	99.86089	93.70187	99.82192	99.86038	99.67456
1499-1549	99.77026	99.71913	99.44284	99.30802	99.56715	99.24528	98.88068	98.79048	99.6671	99.29115	99.67608	99.77549	95.89463	99.74279	99.75901	99.62226
1549-1599	99.70958	99.66684	99.47801	99.37015	99.51653	99.3545	98.46757	99.00169	99.60972	99.31301	99.69045	99.71814	98.22854	99.6771	99.77702	99.60466
1599-1649	99.68787	99.51258	99.32217	99.27687	99.03745	99.19418	96.82662	98.72147	99.48363	98.9527	99.60143	99.61785	97.38053	99.47815	99.6806	99.4826
1649-1699	99.59439	99.55646	99.37	99.31538	99.23567	99.26321	97.63003	98.7643	99.56317	99.14593	99.60787	99.67023	98.05086	99.56656	99.72203	99.53915
1699-1749	99.64388	99.39264	99.43768	99.35689	99.56157	99.36693	98.98172	98.94931	99.64816	99.42277	99.6487	99.72665	99.30022	99.66323	99.74009	99.54666
1749-1799	99.66738	99.4411	99.44324	99.34623	99.63092	99.36812	99.26208	98.95304	99.61947	99.46301	99.64287	99.75844	99.46072	99.63415	99.68772	99.52213
1799-1849	99.64316	99.55458	99.41271	99.34598	99.58953	99.37945	99.21517	98.96735	99.56755	99.46026	99.62381	99.74762	99.50671	99.58537	99.63085	99.49352
1849-1899	99.6286	99.5865	99.38302	99.33931	99.55349	99.37111	99.16688	98.92624	99.52473	99.3992	99.59363	99.69642	99.4192	99.51974	99.57696	99.44681
1899-1949	99.56683	99.58024	99.27227	99.24751	99.45453	99.31676	98.99258	98.75253	99.46228	99.36529	99.49854	99.63486	99.29412	99.41175	99.49974	99.33924
1949-1999	99.58374	99.54804	99.09227	98.98314	99.18891	99.16787	98.4729	98.29215	99.25295	99.1588	99.29827	99.36727	98.89604	99.14968	99.24343	99.3026

Appendix C: FTIR operating procedure

RIN2-FTIR-STANDARD OPERATING PROCEDURE - Modified by Peluso

Shimadzu IR Tracer-100 with AIM 9000 microscope Laboratory: Fascitelli Center for Advanced Engineering 048, RI Consortium of Nanoscience and Nanotechnology (RIN2) Instrument Manager: Dr. Irene Andreu (ian-dreu@uri.edu) 401-874-6885

1. Check the panel on the front of the ATR to make sure that the orange light is illuminated. If the light is not illuminated, contact the instrument manager.

2. Power on: IRTracer-100: press the big, green button on the front panel, right side i. For quantification with the ATR allow the instrument to warm up for 2 hours.

3. Turn on the computer and open LabSolutions IR. There is no password for the software, just click OK

4. To acquire a spectrum, select Spectrum in the LabSolutions IR pop up box

5. Click the Instrument drop down and select Initialize

6. Measurement parameters can be set in the bottom right corner of the Lab-Solutions IR software a. Instrument tab

i. For the Beam Option, choose Internal.

ii. Detector options:

1. Standard-no liquid nitrogen: 350-7800 cm-1

2. Option 1-MCT detector (more sensitive and faster than the standard)-requires liquid nitrogen: 720-5000 cm-1

3. Don't pick options 2 or 3.

iii. The mirror speed needs to be adjusted based on the chosen detector. For the standard detector choose 2.8 or 2.0 (start at 2.8). The MCT detector should be 5 or 9 (typically 9). If the signal to noise ratio is low, you can change mirror speed.

Data

i. For the Measurement mode, we usually select % Transmittance, but that can be adjusted depending on the goals of the analysis.

ii. The Apodization is the algorithm used for converting to the spectrum from the interferogram. Happ-Genzel is the default, but there are other options. The Shimadzu FAQs for FTIR has more information on the other options for apodizations.

iii. Change the number of scans, resolution, and range to the desired values.

7. To measure a sample:

a. Choose a Filename and set the directory in the panel on top of the spectra window. Add a sample name.

b. Compress the ATR arm onto the appropriate background material. Click BKG Scan. The Background spectrum will pop up on the screen.

c. Click Measurement, then choose Sample Scan.

d. Place the material on the ATR crystal and lower the ATR arm into place so it is firmly over the sample.

e. Repeat as necessary for the samples, ensuring that the crystal is cleaned between each acquisition.

8. Post processing

a. An atmospheric correction is performed by the software automatically. This correction removes CO2 and H2O peaks.

b. The atmospheric correction should be performed first and then the ATR correction can be performed.

c. Any processing you do has to be saved manually.

d. Use the Macros to set up several data corrections in a row for multiple samples.

9. To export data, right click on the data and choose Data export. This will export the data as a CSV file.

10. If you are the last user, power down the instrument and the computer. Save your data and close LabSolutions. Push the power button on the IRTracer and flip the switch on the AIM. Liquid nitrogen can be allowed to evaporate from the reservoirs. Make sure that the orange light on the front panel of the IRTracer is still on. If it is not on, contact the instrument manager.

BIBLIOGRAPHY

Baker, L., and Neill, O., 2017, “Geochemistry and mineralogy of a saprolite developed on Columbia River Basalt: Secondary clay formation, element leaching, and mass balance during weathering,” *American mineralogist*, v. 102, p. 1632-1645

Banerjee, S., and Joshi, S., 2013, “Insights into Cave Architecture and the Role of Bacterial Biofilm,” *Proceedings of the Natural Academy of Science, India, Section B Biological Sci.* v. 83, p. 277–290

Baque, M., et al., 2013, “The BOSS and BIOMEX space experiments on the EXPOSE-R2 mission: endurance of the desert cyanobacterium chroococcidiopsis under simulated space vacuum, Martian atmosphere, UVC radiation and temperature extremes,” *Acta astronautica*, v. 91, p. 180-186

Bethke, C., 2011, Geochemical and biogeochemical reaction modeling (second edition), Cambridge university press

Billi, D., et al., 2011, “Damage escape and repair in dried Chroococcidiopsis spp. from hot and cold deserts exposed to simulated space and Martian conditions,” *Astrobiology*, v. 11, n. 1

Billi, D., 2018, “Desert cyanobacteria under space and planetary simulations: a tool for searching for life beyond Earth and supporting human space exploration,” *International journal of astrobiology*, v. 18, p. 483-489

Billi, D., et al., 2019, “Dried biofilms of desert strains of chroococcidiopsis survived prolonged exposure to space and Mars-like conditions in low Earth orbit,” *Astrobiology*, v. 19

Boston, P. et al., 2001, “Cave biosignature suites: microbes, minerals, and Mars,” *Astrobiology*, v. 1, p. 25-55

Boynton, W., et al., 2009, “Evidence for calcium carbonate at the Mars Phoenix Landing Site,” *Science,* v. 325, p. 61–64

Bruggemann, J., et al., 2023, “Structural dependence of extended amide III vibrations in two-dimensional infrared spectra,” *Journal of physical chemistry letters*, v.14, p. 9257-9265

Cady, S., and Farmer, J., 1996, “Fossilization processes in siliceous thermal springs: trends in preservation along thermal gradients,” *Evolution of Hydrothermal Ecosystems on Earth (and Mars?)*, Ciba Foundation Symposium 202, New York, p. 150–173

Cheeptham, N., et al., 2013, “Cure from the cave: volcanic cave actinomycetes and their potential in drug discovery,” *International Journal of Speleology*, v. 42, p. 35-47

Chen, Y., et al., 2013, “Functional groups characteristics of EPS in biofilm growing on different carriers,” *Chemosphere*, v. 92, p. 633-638

Cheptsov, V., 2018, “Microbial activity in Martian analog soils after ionizing radiation: implications for the preservation of subsurface life on Mars,” *AIMS Microbiology*, v. 4, p. 541-562

Chevrier, V., Fitting, A., and Rivera-Valentin, E., 2022, “Limited stability of multicomponent brines on the surface of Mars,” *The planetary science journal*, v. 3

Choudhary, R., et al., 2020, “Impact of forsterite addition on mechanical and biological properties of composites,” *Journal of Asian ceramic societies*, v. 8, p. 1-15

Cockell, C., et al., 2011, “Exposure of phototrophs to 548 days in low Earth orbit: microbial selection pressures in outer space and on early Earth,” *International society for microbial ecology*, v. 5, p. 1671-1682

Cockell, C., Laura C. Kelly and Viggo Marteinsson, 2013, “Actinobacteria—An

Ancient Phylum Active in Volcanic Rock Weathering," *Geomicrobiology Journa*l, v. 30, p. 706-720

Çolak, B., and Güngör, N., 2022, "The Astrobiological Significance of Caves on Earth and on Mars," *International Journal of Environment and Geoinformatics*, v. 9, p. 53-64

Comte, S., Guibaud, G., and Baudu, M., 2006, "Relations between extraction protocols for activated sludge extracellular polymeric substances (EPS) and EPS complexation properties Part I. Comparison of the efficiency of eight EPS extraction methods," *Enzyme Microbiology Technology*, v. 38, p. 237–245

Cuezva, S., et al., 2012, "The biogeochemical role of Actinobacteria in Altamira Cave, Spain," *FEMS microbiology ecology*, v. 81, p. 281–290

Cushing, G. E, et al., 2007, "THEMIS observes possible cave skylights on Mars," *Geophysical research letters*, v. 34

Cushing, G. E., 2012, "Candidate cave entrances on Mars," *Journal of Cave and Karst Studies*, v. 74, no. 1, p. 33–47

Ehlmann, B., et al., 2008, “Orbital Identification of Carbonate-Bearing Rocks on Mars,” *Science*, v. 322, p. 1828-1832

Fairén, A., 2010, “A cold and wet Mars,” *Icarus*, v. 208, p.165-175

Frey, H., et al., 2013, “Slow chemical weathering in a semiarid climate: Changes in the mineralogy and geochemistry of subaerial lava flows in the Deschutes River Basin, central Oregon,” *Chemical geology*, v. 347, p. 135-152

Gislason, S., Veblen, D., and Livi, K., 1992, “Experimental meteoric water-basalt interactions: characterization and interpretation of alteration products,” *Geochimica et cosmochimica*, v. 57, p. 1459- 1471

Groth, I., et al., 2001, “Geomicrobiological study of the Grotta dei Cervi, Porto Badisco, Italy,” *Geomicrobiology,* v. 18, p. 241–258

Hadnott, B., Ehlmann, B., and Jolliff, b., 2017, “Mineralogy and chemistry of San Carlos high-alkali basalts: Analyses of alteration with application for Mars exploration,” *American Mineralogist*, v. 102, p. 282-301

Hart, W., Aronson, J., Mertzman, S., 1984, “Areal distribution and age of low-K, high-alumina olivine tholeiite magmatism in the northwestern Great

Basin," *Geological Society of America Bulletin*, v. 95, p. 186-195

Hassler, D., et al., 2014, "Mars' surface radiation environment measured with the Mars Science Laboratory's Curiosity Rover," *Science*, v. 343, n. 6169

Hays, L., et al., 2017, "Biosignature preservation and detection in Mars analog environments," *Astrobiology*, v. 17, n. 4

Henry, D., Watson, J., and John, C., 2017, "Assessing and calibrating the ATR-FTIR approach as a carbonate rock characterization tool," *Sedimentary geology*, v. 347, p. 36-52

Hughes, S., et al., 2019, "Basaltic Terrains in Idaho and Hawai'i as Planetary Analogs for Mars Geology and Astrobiology," *Astrobiology*, v. 19, n. 3

Kettanah, Y., 2019, "Copper mineralization and alterations in Gercus Basalt within the Gercus Formation, northern Iraq," *Ore Geology Reviews*, v. 111, n. 102974

Kiselev, A., et al., 2006, "Middle Paleozoic basic magmatism of the northwestern Vilyuii rift: composition, sources, and geodynamics," *Petrology*, v. 14, p. 588-608

Kminek, G., and Bada, J., 2006, “The effect of ionizing radiation on the preservation of amino acids on Mars,” *Earth and planetary science letters*, v. 245, p. 1-5

Kopacz, N., et al., 2022, “A Study in Blue: Secondary Copper-Rich Minerals and Their Associated Bacterial Diversity in Icelandic Lava Tubes,” *Earth and space science*, v. 9

Kulkarni, H., et al., 2022, “Geochemical interactions among water, minerals, microbes, and organic matter in formation of speleothems in volcanic (lava tube) caves,” *Chemical Geology*, v. 594

Lavoie, K. et al., 2017, “Comparison of bacterial communities from lava cave microbial mats to overlying surface soils from Lava Beds National Monument, USA,” *PLoS ONE,* v. 12

Leveille, R., Longstaffe, F., and Fyfe, W., 2002, “Kerolite in carbonate-rich speleothems and microbial deposits from basaltic caves, Kauai, Hawaii,” *Clays and clay minerals*, v. 50, n. 4, p. 514-524

Leveille, R., Longstaffe, F., and Fyfe, W., 2007, “An isotopic and geochemical study of carbonate-clay mineralization in basaltic caves: abiotic versus

microbial processes," *Geobiology*, v. 5, p. 235-249

Madejová, J., 2003, "FTIR techniques in clay studies," *Vibrational spectroscopy*, v. 31, p. 1-10

Mangold, N. et al., 2007, "Mineralogy of the Nilli Fossae region with OMEGA /Mars Express data: 2. Aqueous alteration of the crust," *Journal of geophysical research planets*, v. 112

Mathieu, L., 2018, "Quantifying hydrothermal alteration: A review of methods," *Geosciences*, v. 8, n. 245

Matteson, A., and Herron, M., 1993, "End-member feldspar concentrations determined by FTIR spectral analysis," *Journal of sedimentary petrology*, v. 63, p. 1144-1148

Maquelin, K., et al., 2002, "Identification of medically relevant microorganisms by vibrational spectroscopy," *Journal of Microbiology Methods*, v. 51, p. 255-271

Miller, A., et al., 2014, "Siliceous Speleothems and Associated Microbe-Mineral Interactions from Ana Heva Lava Tube in Easter Island (Chile)," *Geomicrobiology journal*, v. 31, p. 236-245

Miller, A., et al., 2018, “Topsoil alterations influence the genesis and composition of unusual organic-rich speleothems in volcanic caves from the Canary Islands,” 19th International conference of humic substances and their contribution to the climate change mitigation 1, Topic 1, Environmental chemistry - dynamics - role of humic substances and natural organic matter.

Morris, R., et al., 2010, “Identification of Carbonate-Rich Outcrops on Mars by the Spirit Rover,” *Science*, v. 329, p. 421-424

Mosca, C., et al., 2019, “Over-expression of UV-damage DNA repair genes and ribonucleic acid persistence contribute to the resilience of dried biofilms of the desert cyanobacterium chroococcidiopsis exposed to Mars-like UV flux and long term desiccation,” *Frontiers in microbiology*, v. 10, n. 2312

Mulder, S., 2023 “Multitechnique characterization of secondary minerals near HI-SEAS, Hawaii, as Martian subsurface analogues,” *Scientific reports*, v. 13, n. 22603

Niles, P., et al., 2012, “Geochemistry of Carbonates on Mars: Implications for Climate History and Nature of Aqueous Environments,” *Space science reviews*, v. 174, p. 301- 328

Northup, D., et al., 2011, “Lava cave microbial communities within mats and secondary mineral deposits: implications for life detection on other planets,” *Astrobiology*, v. 11, p. 601-6182

Popa, R., et al., 2012, “Olivine-respiring bacteria isolated from the rock-ice interface in a lava-tube cave, a Mars analog environment,” *Astrobiology*, v.12, p. 9-18

Popovic, S., et al., 2021, “Endolithic phototrophs: examples from cave-like environments,” *Kragujevac journal of science*, v. 43

Poulet, F., et al., 2005, “Phyllosilicates on Mars and implications for early martian climate,” *Nature*, v. 438

Poulson, T., and Lavoie, K., 2001, “The trophic basis of subsurface ecosystems,” *Ecosystems of the World: Subterranean Ecosystems*, eds Wilkens, H. et al., Elsevier pp. 231–250, New York

Richardson, C., et al., 2012, “Secondary sulfate mineralization and basaltic chemistry of craters of the Moon National Monument, Idaho: Potential martian analog,” *Planetary and space science*, v. 65, p. 93-103

Riquelme, C., et al., 2015, “Actinobacterial diversity in volcanic caves and associated geomicrobiological interactions,” *Frontiers in Microbiology*, v. 6

Rogers, J., and Bennett, P., 2004, “Mineral stimulation of subsurface microorganisms: release of limiting nutrients from silicates,” *Chemical geology*, v. 203, p. 91-108

Roldan., M., and Hernandez-Marine, M., 2009, “Exploring the secrets of three-dimensional architecture of phototrophic biofilms in caves,” *International journal of speleology*, v. 38, p. 41-53

RRUFF database

https://rruff.info/Olivine/R040052

https://rruff.info/diopside/R050406

https://rruff.info/Augite/R061086

https://rruff.info/Anorthite/R040059

https://rruff.info/Calcite/R050127

https://rruff.info/Magnesite/R050676

https://rruff.info/tags=695/R070286

Sallstedt, T., et al., 2014, “Speleothem and biofilm formation in a granite/dolerite cave, northern Sweden,” *International journal of speleology*, v. 43, p. 305-313

Scholl, M., et al., 1990, “The influence of mineralogy and solution chemistry on the attachment of bacteria to representative aquifer materials,” *Journal of contaminant hydrology*, v. 6, p. 321-336

Schorghofer, N., 2021, “Ice caves on Mars: hoarfrost and microclimates,” *Icarus*, v. 357

Schulze-Makuch, D., et al., 2008, “The case for life on Mars,” *International journal of astrobiology*, v. 7, p. 117-141

Simon, K., et al., 2003, “Food web structure and the role of epilithic biofilms in cave streams,” *Ecology,* v. 84, p. 2395–2406

Simon, K., Pipan, T., and Culver, D., 2007, “A conceptual model of the flow and distribution of organic carbon in caves,” *Journal of Cave and Karst Studies,* v. 69, p. 279–284

Srivastava, P., et al., 2018, “Mineralogy and geochemistry of various colored boles from the Deccan volcanic province: Implications for paleoweathering and paleoenvironmental conditions,” Catena, v. 167, p. 44-59

Stegen, J., et al., 2016, “Groundwater-surface water mixing shifts ecological assembly processes and stimulates organic carbon turnover,” *Nature Communications,* v. 7, n. 11237

Tangari, A., et al., 2020, “Volcanic Holocrystalline Bedrock and Hydrothermal Alteration: A Terrestrial Analogue for Mars,” *Minerals*, v. 10

Tasaryova, Z., Janousek, V., and Fryda, J., 2018, “Failed Silurian continental rifting at the NW margin of Gondwana: evidence from basaltic volcanism in the Prague Basin (Tepla-Barrandian unit, Bohemian Massif),” *International journal of Earth science*, v. 107, p. 1231-1266

Teehera, K., et al., 2017, “Cryogenic minerals in Hawaiian lava tubes: a geochemical and microbiological exploration,” *Geomicrobiology journal*, v. 35, p. 227–241

Viramonte, J., et al., 1999, “Cretaceous rift related magnetism in central-western South America,” *Journal of South American earth sciences*, v. 12, p. 109-121

Weng, M., et al., 2022, “Life Underground: Investigating Microbial Communities and Their Biomarkers in Mars-Analog Lava Tubes at Craters of the Moon National Monument and Preserve,” *JGR planets*,

v. 127

Weir, C., and Lippincott, E., 1961, “Infrared studies of aragonite, calcite, and vaterite type structures in the borates, carbonates, and nitrates,” *Journal of Research of the National Bureau of Standards A. Physics and Chemistry*, v. 65A, p. 173-183

Williams, K., et al., 2010, “Do ice caves exist on Mars?,” *Icarus*, v. 209, p. 358–368

Wilson, M., 2004, “Weathering of the primary rock-forming minerals: processes, products and rates,” *Clay Minerals*, v. 39, p. 233-266

Yadev, K., et al., 2021, “Actinobacteria interventions in plant and environment fitness,” Microbiomes and plant health, Academic Press, p. 397-427

2024

IMPLICATIONS OF WATER-ROCK REACTIONS IN LAVA TUBE ENVIRONMENTS AT LAVA BEDS NATIONAL MONUMENT

Jessica Peluso
University of Rhode Island, jpeluso@uri.edu